ORNL/TM-5710

High Energy (E ≤ 1000 GeV) Intranuclear Cascade Model for Nucleons and Pions Incident on Nuclei and Comparisons with Experimental Data

H. W. Bertini
A. H. Culkowski
O. W. Hermann
N. B. Gove
M. P. Guthrie

OAK RIDGE NATIONAL LABORATORY
OPERATED BY UNION CARBIDE CORPORATION FOR THE ENERGY RESEARCH AND DEVELOPMENT ADMINISTRATION

DISCLAIMER

Printed in the United States of America. Available from
National Technical Information Service
U.S. Department of Commerce
5285 Port Royal Road, Springfield, Virginia 22161
Price: Printed Copy $4.50; Microfiche $3.00

ORNL/TM-5710

Contract No. W-7405-eng-26

Neutron Physics Division

HIGH ENERGY ($E \leq 1000$ GeV) INTRANUCLEAR CASCADE MODEL FOR NUCLEONS AND PIONS INCIDENT ON NUCLEI AND COMPARISONS WITH EXPERIMENTAL DATA

H. W. Bertini
A. H. Culkowski*
O. W. Hermann*
N. B. Gove*
M. P. Guthrie

Date Published - August 1977

*Computer Sciences Division

OAK RIDGE NATIONAL LABORATORY
Oak Ridge, Tennessee 37830
operated by
UNION CARBIDE CORPORATION
for the
ENERGY RESEARCH AND DEVELOPMENT ADMINISTRATION

THIS PAGE

WAS INTENTIONALLY

LEFT BLANK

Table of Contents

HIGH ENERGY (E < 1000 GeV) INTRANUCLEAR CASCADE MODEL FOR NUCLEONS AND PIONS INCIDENT ON NUCLEI AND COMPARISONS WITH EXPERIMENTAL DATA

H. W. Bertini and M. P. Guthrie
Neutron Physics Division, Oak Ridge National Laboratory
Oak Ridge, Tennessee 37830

A. H. Culkowski, O. W. Hermann, and N. B. Gove
Computer Sciences Division, Oak Ridge National Laboratory
Oak Ridge, Tennessee 37830

Abstract

An intranuclear cascade model for reactions of pions and nucleons with complex nuclei that should cover the energy range from about 50 MeV to about 1000 GeV has been developed. The model includes the effect of a diffuse nuclear surface, the Fermi motion of the bound nucleons within the nucleus, the exclusion principle, a local potential for nucleons, a localized reduction in the density of the nucleus during the development of the cascade, and the sequencing of the events correctly with time. Theoretical results from the model are compared with experimental data over the energy range ∿ 3-1000 GeV. Within the cascade model, the equations that are used to represent the pion multiplicity from the reactions of nucleons and pions with the individual nucleons of the nucleus underestimates the number of shower particles produced by these individual nucleon interactions. In spite of this the predicted number of shower particles escaping from the nucleus, for 100-GeV nuclear interactions, is overestimated by about 25% for light nuclei to about 60% for heavy nuclei. The agreement for the number of escapes from the nucleus is somewhat better at lower interaction energies

(∿ 10-20 GeV). Some of the major trends in the observed high energy data are predicted quite well. These include the energy independence of (a) the number of black tracks produced at interaction energies above 5 GeV, (b) the number of shower particles produced above 100 GeV, and (c) the radionuclides produced above 10 GeV. Other trends that are predicted fairly well are the small mass dependence of the shower particle multiplicity (factor of 2 increase predicted from carbon to lead, factor of 1.5 measured), and the change in the angular dependence of the multiplicity with mass. In absolute comparisons, the predicted total reaction cross sections are in good agreement with experimental data, and the cross sections for the production of radionuclides are in fair agreement.

INTRODUCTION

The interaction of nucleons and π-mesons at high energies (∿ 100 GeV) with nuclei is calculated using the intranuclear cascade approach with a computer program called HECC-1. In this approach the transitions to the continuum states of the final residual nuclei from the interaction of a high-energy particle with a target nucleus is determined by calculating the individual life histories of the incident particle, and all subsequent collision products, as they travel through the nucleus and interact with the bound nucleons therein. A cascade of particles is thus generated within the nucleus. The interactions with the bound nucleons are considered to be free particle interactions modified by exclusion effects. These free particle reactions include scattering, charge exchange scattering (for π-nucleon reactions), production of π-mesons, and pion absorption.

Monte Carlo techniques are used to specify all of the variables needed to determine the life histories. The nucleus is left in a highly excited state after the completion of the cascade, and an evaporation calculation is employed to permit the deexcitation of the nucleus.[2]

The method differs from that reported previously[3,4] in that the cascade events that are assumed to occur inside the nucleus are properly sequenced in time whereas in the previous work this was not the case, and the local nuclear density in the vicinity of a cascade collision is reduced to account for the removal of a nucleon from the Fermi sea. In the earlier work the reduction of the nuclear density as the cascade developed was ignored.

Various trends in the interaction of high energy nucleons and pions with nuclei have been discerned and summarized recently[5], and the ability of the model to predict these trends along with other comparisons with experimental data will be examined. All of the calculated results shown below are in absolute units unless specified otherwise.

OTHER APPROACHES

Other approaches in the calculation of very high energy nuclear reactions are under study. One is the multiperipheral model[6] in which a series of particles of decreasing rapidity (the rapidity $y = \frac{1}{2} \ln[(E+p_z)/(E-p_z)]$) are emitted until a particle with rapidity equal to that of the target interacts with the target. Given a characteristic time T_0, in the rest frame of the particle, it is assumed that only those particles can interact with the nucleons of the nucleus if in time T_0 they have not passed the nucleus. Thus, only the last of the

particles in the emitting chain can interact with the nucleus. The effect of the model is to enhance the rapidity distribution for a nuclear reaction, compared to that for hadron-hadron reactions, only at the low end of the rapidity scale. This is in conformity with some of the broad features of the experimental data.[5]

Another model that qualitatively yields the same rapidity distribution is the energy flux cascade model.[7] A hadron nucleon collision within the nucleus is assumed to form an excited hadronic state, the energy flux, which instantaneously acquires a rapidity distribution that is the same as the asymptotic distribution of produced particles in a hadron-hadron collision. As time proceeds the distribution spreads out in space with the faster part of the distribution in the front and the slower part at the end. When any part of the distribution reaches a spatial size equal to that of a single hadron, it behaves as a single hadron with a rapidity equal to the average rapidity of that part of the distribution. In approximately one mean free path within the nucleus the front part of the distribution has sufficiently spread to be considered as a single hadron which interacts with another nucleon. The remaining part has a lower energy, and it produces negligible multiplicity upon interacting with a nucleon. The process continues in this manner with new energy flux created at the end of each mean free path.

Another approach is the conglomerate model[8] in which it is assumed that the interaction time is so long that all of the nucleons in the path of the incident particle are involved as a conglomerate which decays outside of or independently of the nucleons remaining. This will move the tailing end of the rapidity distribution backward in the lab. frame, which again roughly corresponds to the observed data.

The last model to be discussed is an intranuclear cascade calculation developed by Artikov *et al.*[9] In this version the nucleons in the nucleus are assigned fixed locations within the nucleus, and they are distributed such that their density is uniform throughout the nucleus. The nucleus is given a random rotation for the calculation of each incident particle. During the calculation of the cascade, when the trajectories of more than one cascade particle terminate at or near the position of a fixed nucleon within the nucleus, these cascade particles all interact simultaneously with the single, fixed nucleon (many-particle interaction). Although fixed in space the struck nucleon is allowed to have a momentum governed by a zero termperature Fermi distribution. The energy available to produce pions from this many-particle interaction is the "free energy", ε, where

$$\varepsilon = [(\sum_i E_i)^2 - (\sum_i \bar{p}_i)^2]^{\frac{1}{2}} - \sum_i m_i$$

with E, p, and m, representing the total energy, momentum, and mass of the particles involved. The energy and angular distribution of the secondary particles are taken from the energy dependent experimental data of secondary particles produced from nucleon-nucleon reactions.

When only one cascade trajectory terminates in the vicinity of a fixed nucleon, the reaction is calculated as a free-particle reaction where scattering and pion-production reactions are included. In all cases exclusion effects are included, and also calculations were carried out with and without the effects of a "leader" particle, i.e., a single particle that carries off most (50-70%) of the available energy. Those fixed nucleons that are struck are removed from the sea of fixed nucleons and hence a local void is created.

Comparisons with experimental data indicate that the leader particle, when employed, creates an excessive number of shower particles at reaction energies of $\sim$ 100 GeV. At lower energies ($E \leq 30$ GeV) only small differences in results with or without it are ascertained. A better agreement with experimental data is obtained when many-particle interactions are included.

The intranuclear cascade model described in this paper differs in that no multiparticle reactions are considered and effects of a leader particle are not included. The time sequence of events is taken into account whereas it is not by Artikov *et al.*, and both include the effects of the reduction of nuclear density at each interaction site within the nucleus.

MODEL OF THE NUCLEUS

Detailed descriptions of the properties of the nucleus that are taken into account are given elsewhere.[3,10] Changes from the earlier versions that have been incorporated will be described in some detail. The model nucleus can be divided into a maximum of 50 spherical annuli. Each annulus can further be divided by 50 planes all intersecting along the z axis and equally spaced from each other in angle, and 50 cones that originate at the origin and for which the z axis is the axis of symmetry. Each annulus can be subdivided into planes and cones independently of the other annuli. However, the memory space within the computer program that is allocated to carry all of the information required for the cascade-particle histories would probably be exceeded if the maximum numbers of subdivisions were used. In our experience the program will accommodate a total of 300 subdivisions (regions) of the

nucleus without exceeding the cascade-particle memory requirements. All regions within a spherical annulus have the same density, but the density decreases from annulus to annulus from the center to the outer boundary.[10]

The effects of a spatially dependent potential are included for nucleons[10], but not for pions. The Fermi motion of the bound nucleons and the effects of the exclusion principle are taken into account.[3,10] Reflection and refraction[11] and nuclear correlations[12] are not included. The latter is included only in that pion absorption is assumed to take place with nucleon-nucleon pairs within the nucleus.[10]

The sampling technique that was used to select the momentum of the struck nucleon is described in another report.[13]

PARTICLE-PARTICLE INPUT DATA

All nucleon-nucleon cross sections at energies below 3.5 GeV and all pion-nucleon cross sections at energies below 2.5 GeV were taken to be the same as those used in the lower energy version of the calculation (MECC-7)[4]. At higher energies the particle-particle cross sections that were used are illustrated in Figs. 1-4. The n-n cross section was taken to be the same as the p-p cross section; the π^--n cross section was set equal to the π^+-p cross section, and the $\pi^\pm$-n, π°-n, and π°-p cross sections were arbitrarily set equal to the π^--p cross section. These assignments apply for the differential cross sections as well.

The differential scattering cross section for particle-nucleon scattering at energies greater than 3.5 GeV for incident nucleons and at energies greater than 2.5 GeV for incident pions was represented by

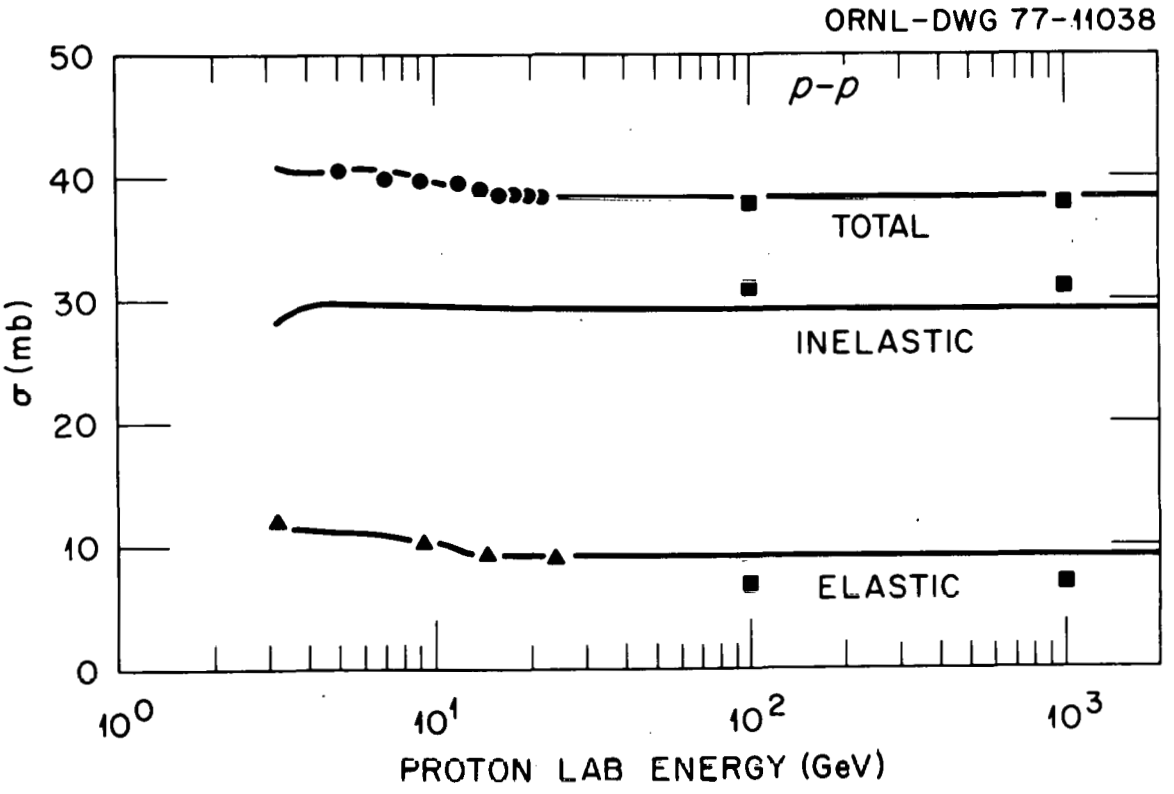

Fig. 1. High energy p-p cross sections. Solid lines are the cross sections used in the calculation.

- ● W. Galbraith *et al.*, Phys. Rev. 138, B913 (1965);
- ■ L. V. Vokova, Bull. Acad. Sci. USSR, Phys. Series 31, 1508 (1967) (theoretical prediction);
- ▲ G. Alexander *et al.*, Nucl. Phys. B5, 1 (1965).

When not shown, experimental error bars are smaller than the symbols.

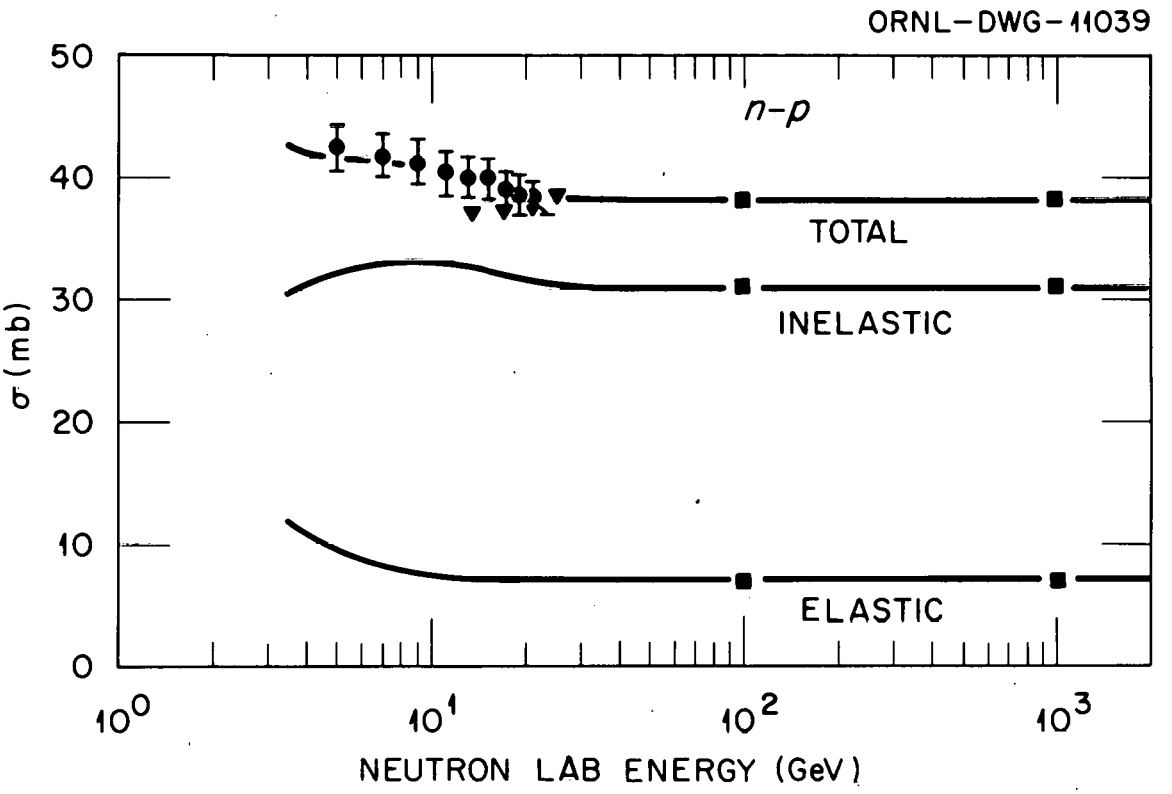

Fig. 2. High energy n-p cross sections.
▼ M. N. Kreisler *et al.*, Phys. Rev. Letters 20, 468 (1968).
All else as in Fig. 1.

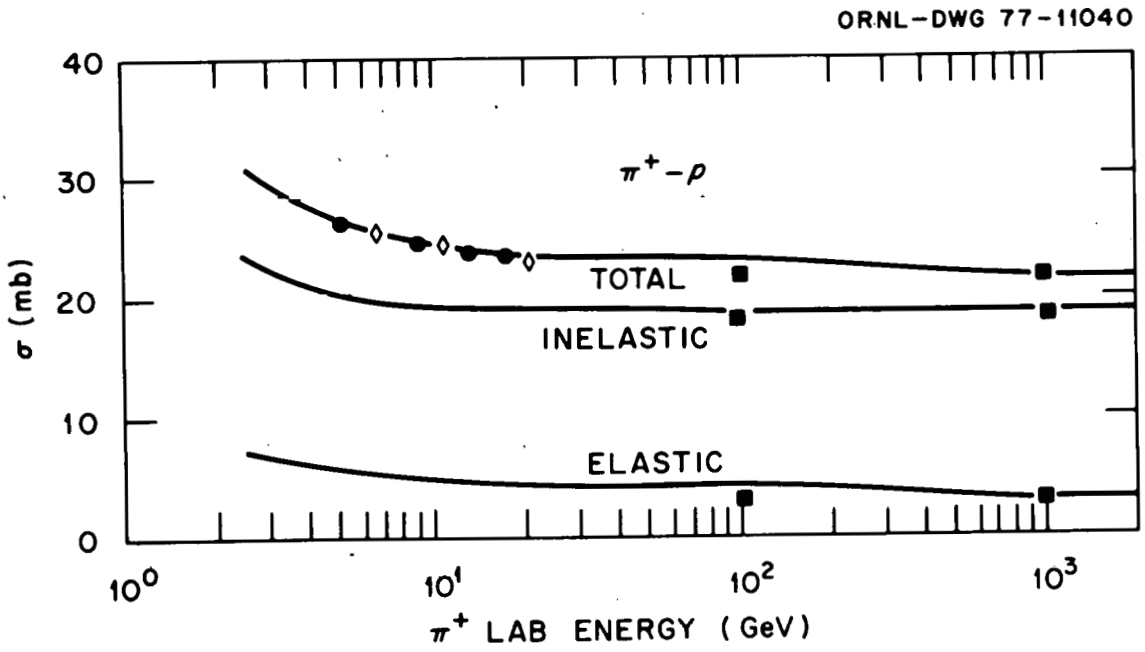

Fig. 3. High energy π^++p cross sections.
◊ K. J. Foley *et al.*, Phys. Rev. Letters 19, 330 (1967).
All else as in Fig. 1.

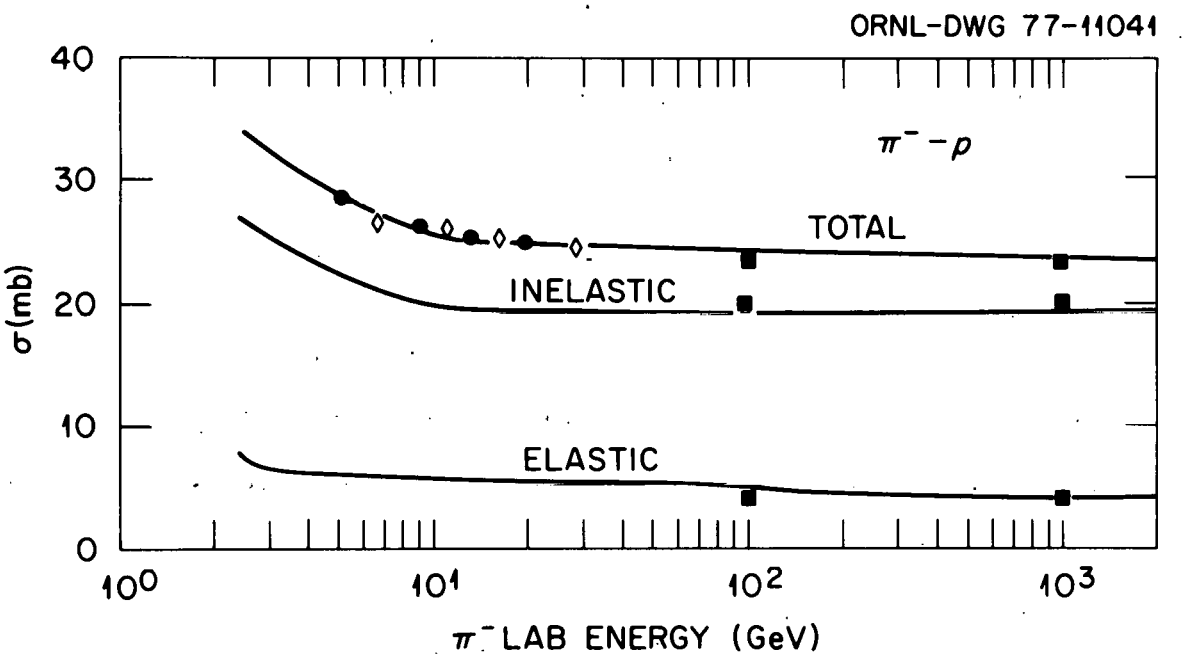

Fig. 4. High energy π^-+p cross sections. Symbols defined in Figs. 1 and 3.

$$\frac{d\sigma}{dt} = \exp\,(A - B|t|)\ ,$$

where t is the square of the 4-momentum transfer in the center of momentum (cm) system, and it is related to the scattering angle in this system by

$$\cos\,\Theta_{cm} = 1 - \frac{|t|}{2K^2}\ .$$

K^2 is the square of the 3-momentum of either particle in the cm system before or after scattering with

$$K^2 = \frac{M^4 - 2M^2(m_1^2+m_2^2)+(m_1^2-m_2^2)^2}{4M^2}\ ,$$

where M is the total energy in the cm system and m_1 and m_2 are the rest masses of the particles involved in the collision. The constant A was used only for normalization purposes. For nucleon-nucleon scattering the parameter B was taken to be

$$B = 7.26 + .0313\ p_o\ ,$$

where p_o is the momentum of the incident particle. This representation of the parameter B compared to the values obtained when experimental cross section data[14] were fit by $\frac{d\sigma}{dt} = \exp[A-B|t|]$ are shown in Fig. 5.

For π^+-p and π^- - p scattering the values of B were taken to be constant at 7.575 and 7.04, respectively. These are the average values of those reported in Ref. 15 which were obtained by fitting experimental data over the energy range from 8.5 to 18.4 GeV/c.

The sampling technique that was used to specify the scattering angles in the cm system is described in Appendix B.

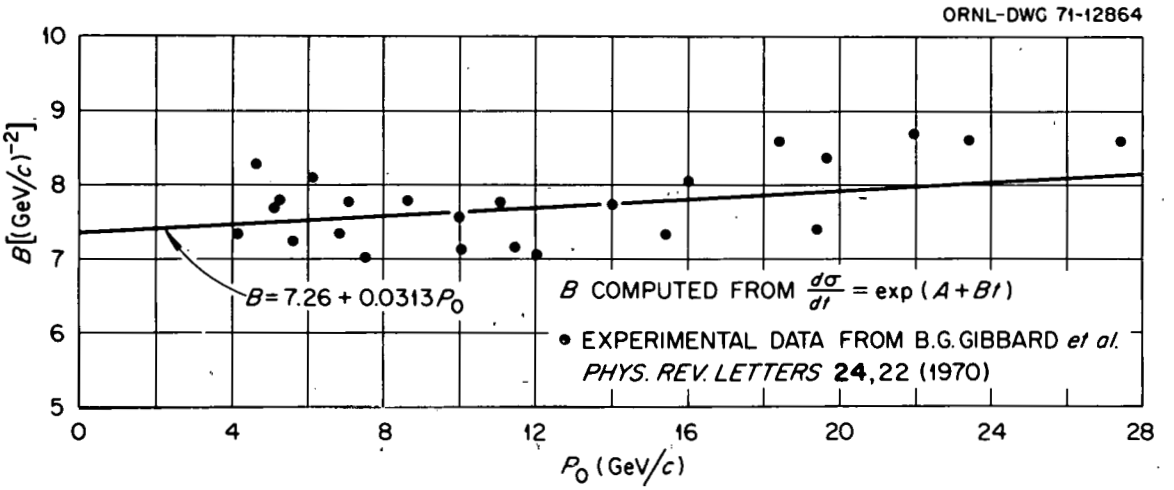

Fig. 5. Parameter B for the differential nucleon-nucleon scattering cross section vs the momentum of the incident particle in the lab system.

THE CALCULATION

Since adequate descriptions of the general approach to the calculation of nuclear reactions by the method of intranuclear cascades have appeared in the literature[1,9-13], only those features of the calculation that are different from the version that applies at lower energies[4] will be described here.

Time Sequence of Events

One of the features of the present model that is different from the intranuclear cascade model reported previously[3,4] is that the cascade events are properly sequenced in time. The time, t, is set to zero when the incident particle has made a collision. Two time values are associated with every particle that makes up the cascade. One is the time at which the particle will make the next collision, t_c, and the other is the time that the particle will cross the boundary of the region in which it is located, t_b. Both t_c and t_b are measured from t = 0, when the cascade was initiated. The time-to-the-boundary crossing is calculated as though no collision were scheduled to take place within the region. Whether this will be true or not depends on whether the sampled site of the next collision lies outside or inside of the region. The time between events (either boundary crossings or collisions) is calculated by dividing the distance between them by the velocity of the particle. The next event, out of all possible events, is determined by the smallest value of all of the listed t_b's and t_c's.

It was necessary to include boundary crossings as events so that an account of the effect of a reduction of the density in the regions that

lie in the paths of the cascade particles could be made. In other words, if the density of a region were reduced because of a collision that took place within it at an earlier time, then this reduced density would be used to determine the collision probability within that region for cascade particles that arrived at a later time. When a particle arrives at a boundary, the density of the region that the particle is about to enter is examined to see if it has been reduced. If it has not, the calculation proceeds, and if it has, a new probability for a collision within the region is calculated.

Density Depletion

Each incident particle interacts with an undisturbed nucleus whose density is normalized such that

$$\int(\rho_p+\rho_n)dV = \sum_{i=1}^{R} (\rho_{pi}+\rho_{ni})V_i = A ,$$

where ρ_p and ρ_n are the number of protons and neutrons per cm^3; the subscript i refers to the ith region number; R is the number of regions in the nucleus; and A is the mass number of the nucleus. If a collision in the ith region occurs with a proton (similarly with a neutron), the density in that region is reduced by one proton, i.e.,

$$\Delta\rho_{pi}V_i = 1 ,$$

and the residual density, ρ_{pi}^r, is given by

$$\rho_{pi}^r = \rho_{pi} - \Delta\rho_{pi} .$$

If the residual density is less than zero, the density in that region is set equal to zero, and nuclear matter is subtracted from the nearest-neighbor regions in such a manner that the total reduction in nuclear matter is equal to one proton. This is accomplished by reducing the density of the jth nearest-neighbor region by an amount $\Delta\rho_{pj}$ such that

$$V_j \, \Delta\rho_{pj} = \frac{\rho_{pj} V_j (1-\rho_{pi} V_i)}{\sum_{j=1}^{n} \rho_{pj} V_j} \quad ,$$

where n is the total number of nearest-neighbor regions. If the residual densities of the nearest-neighbor regions are less than zero, their densities are set equal to zero and the deficit in nuclear matter that must be made up to equal 1 proton is subtracted from the next-nearest neighbors in a similar matter.

This procedure is adopted to insure that the depletion of the nuclear matter is localized or centered at the location at which the collision occurred. Nearest-neighbor regions are those that have a bounding surface that partially or completely overlaps a surface of the region in question, and next-nearest-neighbors are those whose corners (loosely speaking) touch the corners of the region.

Multiple Particle Production

At the lower energies ($E \leq 2.5$ GeV for pions and ≤ 3.5 GeV for nucleons) the production of pions in particle-particle reactions is treated in the same manner as was done previously[3,4], i.e., the Lindenbaum Sternheimer isobar model was employed.[16] At higher energies the empirical formulas developed by Ranft were employed to determine

the multiplicities and the spectra of the secondary particles.[17] The creation of all particles other than pions was ignored mainly because pion production is by far the dominant mode.

The equation that described the nucleon spectra from inelastic nucleon-nucleon collisions for a system in which the struck nucleon is at rest is

$$N_{nn}(p,\Theta) = \left(\frac{A}{p_o} + \frac{Bp}{p_o^2}\left[1+\left\{1+\left(\frac{p_o}{m}\right)^2\right\}^{\frac{1}{2}} - \frac{p_o}{p}\left\{1+\left(\frac{p}{m}\right)^2\right\}^{\frac{1}{2}}\right]\right) \times p^2 \times \left(1+\left\{1+\left(\frac{p_o}{m}\right)^2\right\}^{\frac{1}{2}} - \frac{pp_o}{m^2}\left\{1+\left(\frac{p}{m}\right)^2\right\}^{-\frac{1}{2}}\right)\exp[-cp^2\Theta^2], \quad (1)$$

where

$N_{nn}(p,\Theta) \equiv$ No. of nucleons per unit momentum per unit solid angle,

$p \equiv$ Momentum in GeV/c of the secondary nucleons,

$p_o \equiv$ Momentum of the incident nucleon (GeV/c),

$m \equiv$ Rest mass of the nucleon (GeV),

$\Theta \equiv$ Polar angle of the secondary particle (radians),

$A = .55$,

$B = -0.30$,

$C = 2.68$.

The equation for the secondary pion spectra in a nucleon-nucleon collision is

$$N_{n\pi}(p,\Theta) = A_1p^2 \exp\{-A_2pp_o^{-\frac{1}{2}} - A_3pp_o^{\frac{1}{2}}\Theta^2\} + (B_1p^2/p_o)\exp\{-B_2(p/p_o)^2 - B_3p\Theta\}, \quad (2)$$

where p is the momentum (GeV/c) of the secondary pion, p_o the momentum of the incident nucleon, and the constants are taken to be

$$A_1 = 4.75, \qquad B_1 = 3.546,$$
$$A_2 = 3.76, \qquad B_2 = 10.21,$$
$$A_3 = 4.23, \qquad B_3 = 4.28.$$

The normalization of this expression is such that integration over all angles and all secondary particle momentum will give the total pion multiplicity (i.e., the sum of the numbers of secondary π^+, π°, and π^-) for an incident nucleon with momentum p_o. It was arbitrarily assumed that the multiplicity of pions of each charge state was 1/3 the total.

Equations 1 and 2 were found to fit experimental data reasonably well.[18] Equation (2) was arbitrarily used to represent the recoil nucleon and the secondary pion spectra from pion-nucleon inelastic collisions by letting p_o represent the momentum of the incident pion and p the momentum of the recoil nucleon or the secondary pion.

A detailed description of the Monte Carlo sampling technique that is employed for these distribution functions is given in Appendix B. The technique is such that total energy, charge, and baryon number (nucleons in this case) are conserved for each of the individual particle-particle interactions; momentum is not conserved. The secondary particle spectra in these inelastic collisions are determined in the system in which the struck particle is at rest. Momentum non-conservation in this system results in energy non-conservation in the laboratory system when the usual relativistic transformations to the laboratory system are made. Conservation of energy in the lab. system is imposed by renormalizing, i.e., following the transformation to the lab. system, the transformed energy of each particle is multiplied by the ratio of the initial total laboratory energy of the reaction to the sum of the

total energies of all of the particles following the transformation. The magnitude of the momentum of each particle is recalculated to correspond to the renormalized total energy of the particle, but its direction cosines are unchanged from those obtained from the transformation.

EFFECT OF DENSITY DEPLETION AND NUMBER OF REGIONS

The effects on the secondary particle multiplicities of the number of regions used in the calculation, and the effects of nuclear density depletion are illustrated in Figs. 6 and 7. The particle multiplicities are independent of the number of regions used in the model nucleus beyond about 15 regions for Al and 50 regions for Pb. When the number of regions are greater than these values the deviations from a straight line are within the statistics of the results. When nuclear density depletion is not taken into account the effect on the nucleon multiplicity is large at all energies shown, but it is large for the pion multiplicity only at the higher energies. Results for the cases without depletion are independent of the number of regions.

For all of the comparisons illustrated below the number of regions for each target nucleus was taken to be approximately equal to the mass number of the target, and nuclear depletion was included.

COMPARISONS WITH EXPERIMENTAL DATA

Total Nonelastic Cross Sections

Comparisons of the theoretical predictions with the experimental data for $\sim$ 50-GeV pions and protons on various targets are shown in Fig. 8. The agreement is quite good.

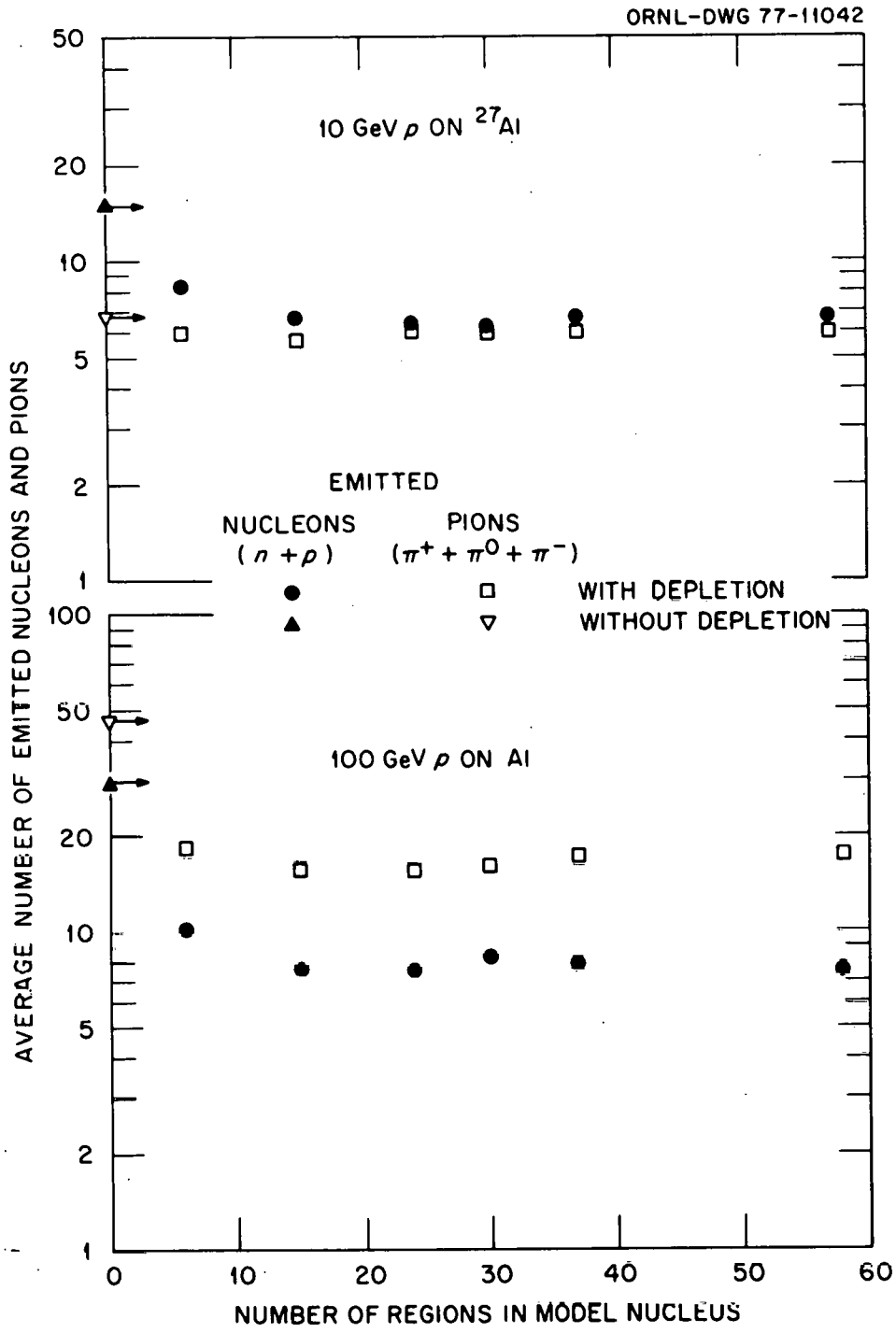

Fig. 6. Average number of emitted nucleons (n+p) and pions ($\pi^+ + \pi^\circ + \pi^-$) per incident particle collisions vs the number of regions used in the model nucleus. The reactions are 10- and 100-GeV p on ^{27}Al. The results for the cases without the inclusion of nuclear density depletion are independent of the number of regions (indicated by the arrows). The statistical error associated with each data point is about the size of the symbol.

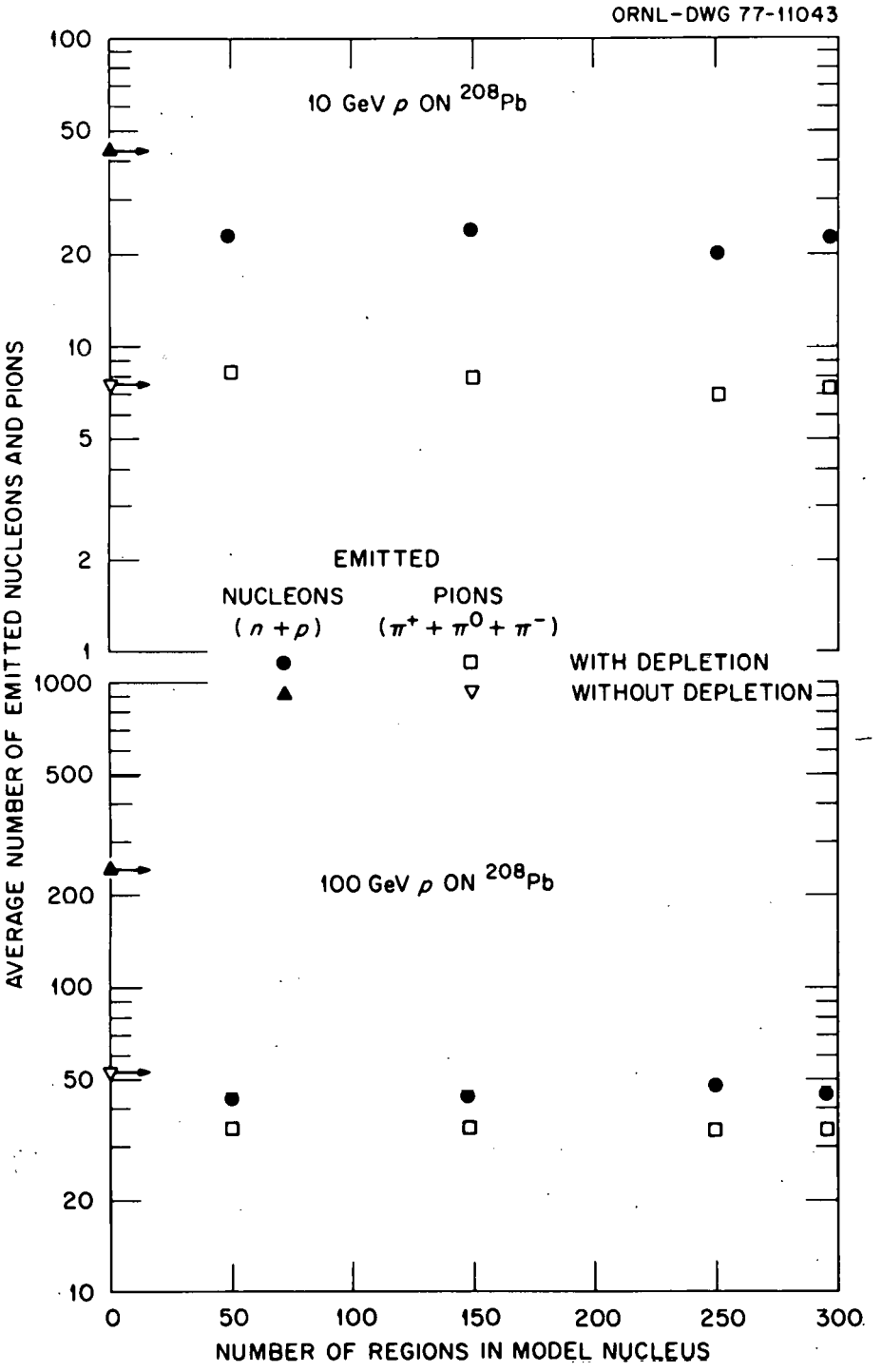

Fig. 7. Same as Fig. 6 for the reactions of 10- and 100-GeV p on ^{238}U.

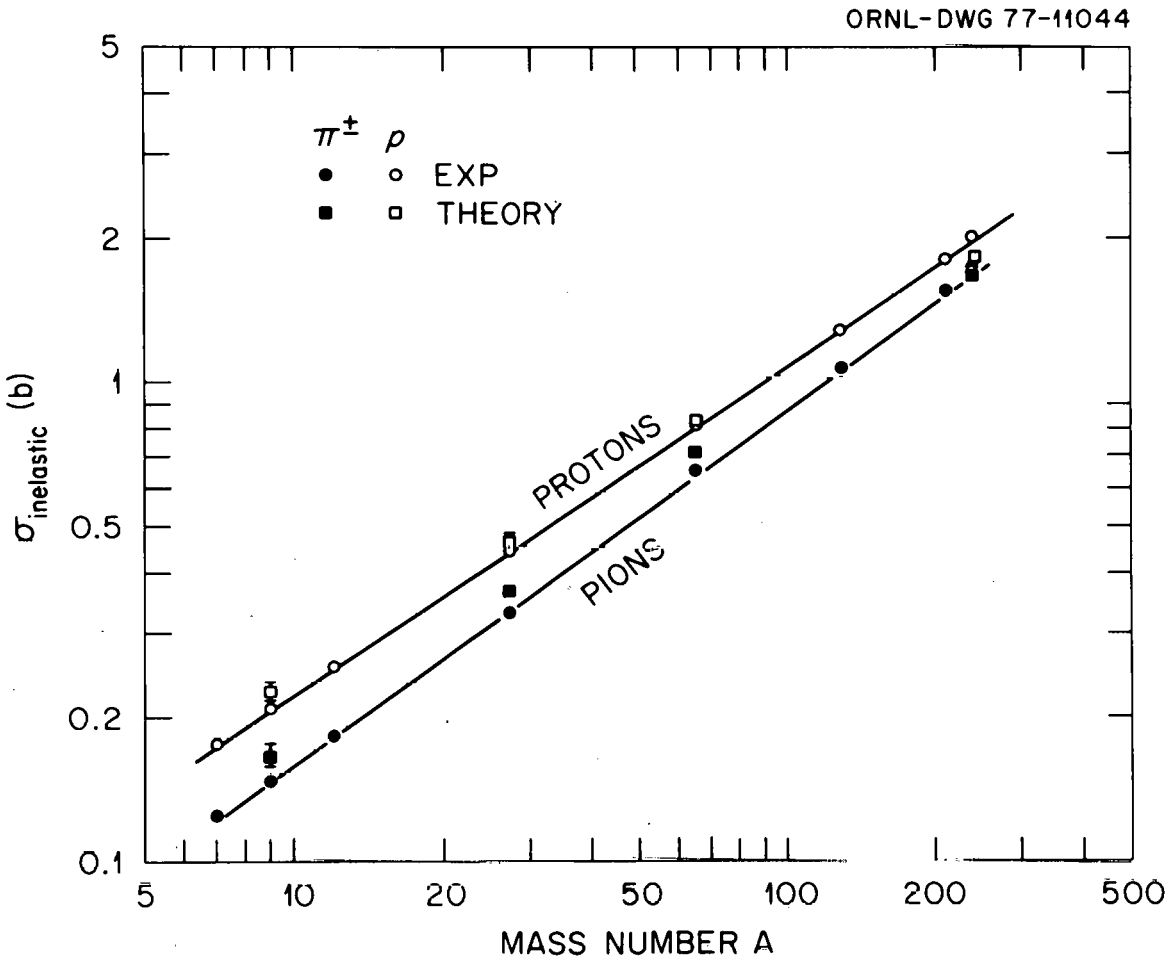

Fig. 8. Experimental and theoretical total inelastic cross sections for incident protons and pions on various nuclei. The experimental data are for incident 30-70 GeV $\pi^{\pm}$ and protons (S. P. Denisov *et al.*, Nucl. Phys. B61, 62 (1973), quoted by Busza, Ref. 5). The calculated results are for incident 50-GeV $\pi^{\pm}$ and protons. Where not illustrated, the statistical error on the calculated results are of the order of the size of the symbols. Solid lines were drawn through the experimental data merely to guide the eye.

Particle Multiplicities

Comparisons between theoretical predictions and experimental data for the secondary particle multiplicities have been made on an absolute basis, i.e., comparing absolute numbers of particles produced from the reactions, and on a relative basis, i.e., comparing ratios of particles produced from the nuclear reactions to numbers of particles produced from p-p reactions.

Absolute Multiplicities

Fig. 9 illustrates comparisons between experimental emulsion data[19] and predictions from the calculation for incident π^- at various energies. The target used for the theoretical results was bromine-80 which was assumed to be representative of the constituents of the emulsion. The theoretical shower particle data are taken to be the average numbers of π^+ and π^- produced with $\beta \geq 0.7$ ($\sim$ 56 MeV) per interaction, and the theoretical numbers representing black tracks are the sums of the average numbers of ^1H, ^2H, ^3H, ^3He, and ^4He that were evaporated following the cascade.

Even though they are fairly standard these theoretical assignments of shower particles and black tracks are somewhat arbitrary because the exact nature of the particles that are measured is ill-defined. Unfortunately, this lack of definition causes explanations of discrepancies between experimental results and theoretical predictions to be somewhat speculative in that the discrepancies may be partly due to a comparison of different entities rather than different values of the same entity.

Assuming that the theoretical assignments represent the quantities measured, the greatest discrepancies ($\sim$ 50%) between the predictions and

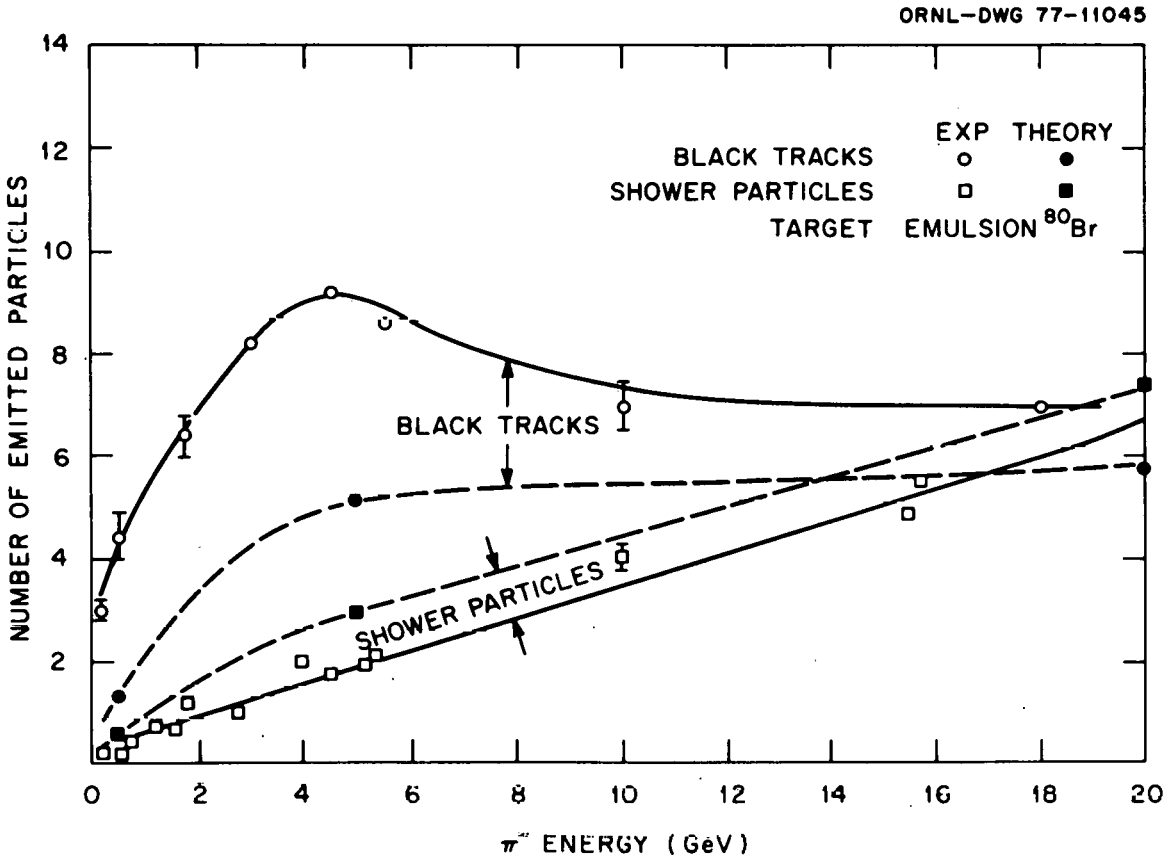

Fig. 9. Average number of shower particles and black tracks vs incident pion energy for π^- on emulsions. Experimental data quoted by V. S. Barshenkov, K. K. Gudima, and V. D. Toneev, Octa Physica Pol. 36, 457 (1969). Theoretical results are from π^- on bromine-80. Solid and dashed lines are drawn through the experimental and theoretical data respectively merely to guide the eye. See text for details.

the experimental data occur at about 4 GeV or lower for both the black tracks and the shower particles. At the highest energies the discrepancies are about 15%. The agreement of the theoretical results with the experimental data may be considered to be fair or poor.

However, at this stage of the development of the theoretical model the predicted trends in the energy dependence of the results in comparison with the experimental trends are about as important as the comparisons of the absolute values themselves. In this regard, the predicted trends are in excellent agreement with the experimental data. Since it is generally assumed that the black tracks are largely the result of the evaporation mechanism, and the number of black tracks is dependent on the excitation energy of the evaporating nucleus, both the experimental data and the theoretical predictions indicate the onset of a saturation effect for the excitation energy at about the same incident particle energy.

Relative Multiplicities

A comparison between the experimental data[5] and the theoretical predictions for the ratio of shower particles produced in emulsions to those produced in p-p collisions vs incident proton energy is shown in Fig. 10. The experimental shower-particle data at incident particle energies greater than 300 GeV are from cosmic rays. The theoretical data are for incident protons on bromine-80, and the theoretical shower particles are as described in the previous section. The predicted ratios are high by factors of 4 and 5. Table I contains the theoretical results from which the data in Fig. 10 were obtained.

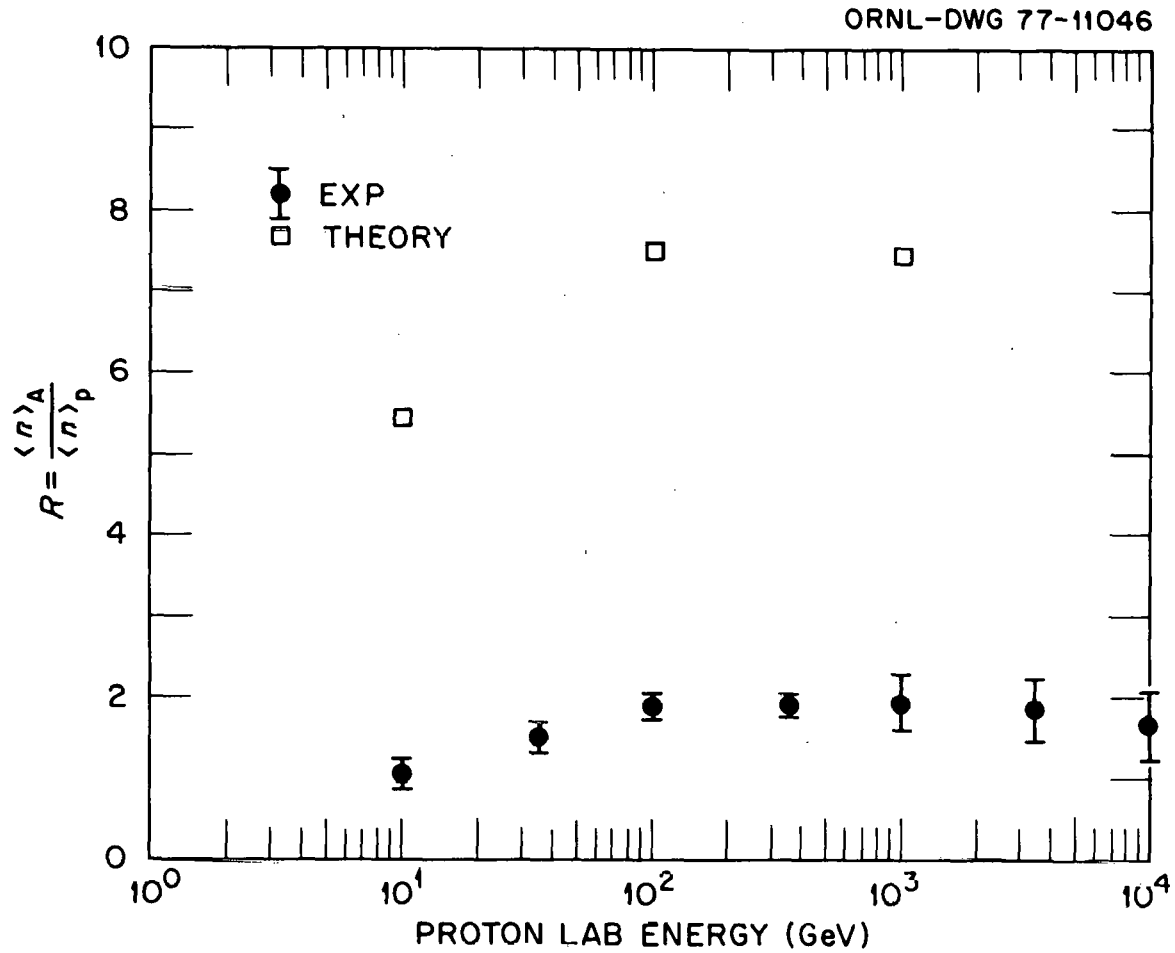

Fig. 10. Ratio of the number of shower particles produced by protons on emulsion to those produced by p-p collisions vs incident proton energy. Experimental data quoted by W. Busza, A. I. P. Conference Proceedings No. 26, "High Energy Physics and Nucl. Structure - 1975" (p. 211). The statistical errors associated with the theoretical results are about the size of the symbols. See text for details.

Table I. Theoretical values for the sum of π^+ and π^- with $\beta \geq 0.7$ emitted per interaction for incident protons

Inc. Proton energy[a] [GeV or GeV/c]	Target	
	p[b]	Br
10	0.70	3.8 ± 0.1
100	1.88	14.2 ± 0.3
1000	5.50	41.0 ± 0.7

[a]For p-p interactions, the units are GeV/c. For reactions with the complex nuclei, the units are GeV.

[b]These are the values obtained by taking 2/3 of the results when Eq. (2) is integrated over angle and over secondary pion momenta.

Table II. Theoretical and experimental[a] shower particle multiplicities from reactions of π^- on nuclei

Inc. Pion Energy	Target							
	P		C		Cu		Pb	
	Exp.	Theor.[b]	Exp.[c]	Theor.	Exp.[c]	Theor.	Exp.[c]	Theor.
100	6.5±0.4	1.88	8.4±0.7	10.4±0.1	10.6±0.9	14.7±0.1	12.6±1.1	20.1±0.3
175	7.7±0.5							

[a]W. Busza *et al.*, Phys. Rev. Letts. 34, 836 (1975).

[b]See footnote b, Table I.

[c]Results shown are the average values from 100 and 175 GeV inc. π^-. These data were calculated from the values given in column 2 and those shown in Fig. 11, all of which were taken from Ref. a.

Similar discrepancies appear when the ratio is plotted vs mass number, as is illustrated in Fig. 11. The theoretical results are from 100 GeV π^- on C, Cu, and Pb, and the experimental data are the average values from 100 and 175 GeV incident π^- on the elements shown and for shower particles with $\beta \geq 0.85$ ($\sim$ 125 MeV pions)[20]. Table 2 shows the data before the ratios were calculated where it is apparent that the theoretical model used to represent the reactions with protons underestimates the multiplicities by more than a factor of 3. In spite of this, the predicted multiplicities from reactions with nuclei are larger than the experimental values by 25 to 60%.

The implications from these comparisons are that the theoretical nuclear reaction model enhances the shower particle production by the factors illustrated in Figs. 10 and 11. However, it does not necessarily follow that the same enhancement would be maintained if a more realistic pion-nucleon model were employed, and the reason is that if 3 times more particles (for example) are created in the initial collision with a nucleon inside the nucleus the average energy of these particles will be about a factor of 3 less. On subsequent collisions inside the nucleus these particles will create fewer particles than is presently the case. Verification of this thesis must await the implementation of a more realistic particle-nucleon model into the calculation, but such implementation will require a substantial effort.

As with the comparisons in the previous section, the important energy dependence of the results from the model, shown in Fig. 10, is in excellent agreement with that demonstrated by the experimental results, i.e., the theoretical model achieves a "saturation effect" of the shower

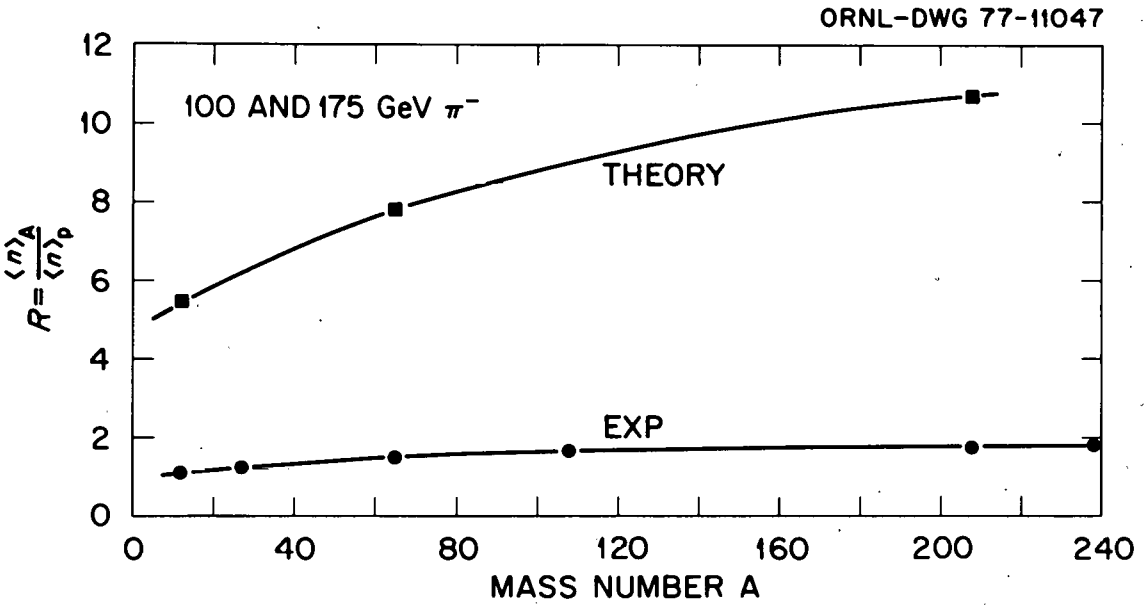

Fig. 11. Ratio of number of shower particles produced for various targets to those produced for a proton target. Experimental data are the average values from 100 and 175 GeV incident π^-, and the error bars are smaller than the symbols. [W. Busza *et al.*, Phys. Rev. Letters 34, 836 (1975)]. Theoretical results are for incident π^- at 100 GeV, and the statistical errors are about the size of the symbols. Solid line curves are drawn through the experimental and theoretical data merely to guide the eye.

particle multiplicity at about the same energy as do the actual reactions. The predicted mass dependence of the multiplicity, Fig. 11, varies by about a factor of 2 from C to Pb while it varies by about 1.5 over the same mass range for the experimental data.

As pointed out by Busza, the most striking feature of the experimental data, both from counters and emulsions, is that the increase in the multiplicity with nuclear mass number occurs entirely at large angles[5]. There is no discernable enhancement of the multiplication in the forward direction with mass number. The theoretical results for various angular intervals are shown in Table 3. There is no increase in the multiplicity over the mass range from C to Pb in the angular interval 0-3.5°, while there is a successively larger increase as larger angles are considered. For the data shown, the largest increase is for the angular interval 26-110, hence the "striking" feature of the experimental data is predicted by the model. These angular intervals were selected to conform to those used in recent experiments.[20] Direct comparison with experimental data is somewhat difficult because this data was reported only in the form of ratios of multiplicities from nuclei to those from protons, and, as discussed above, the theoretical model predicts these ratios to be large. Compounding the difficulty is the fact that the theoretical model representing the reactions with nucleons yields only $\sim$ 1% of the total multiplicity in the last angular interval (26-110°) and, as a result, the theoretical ratios calculated for this angular interval, where the 1% value is used in the denominator, are very large. An attempt to compare the predicted ratios with the experimental data is shown in Fig. 12 where all of the theoretical ratios

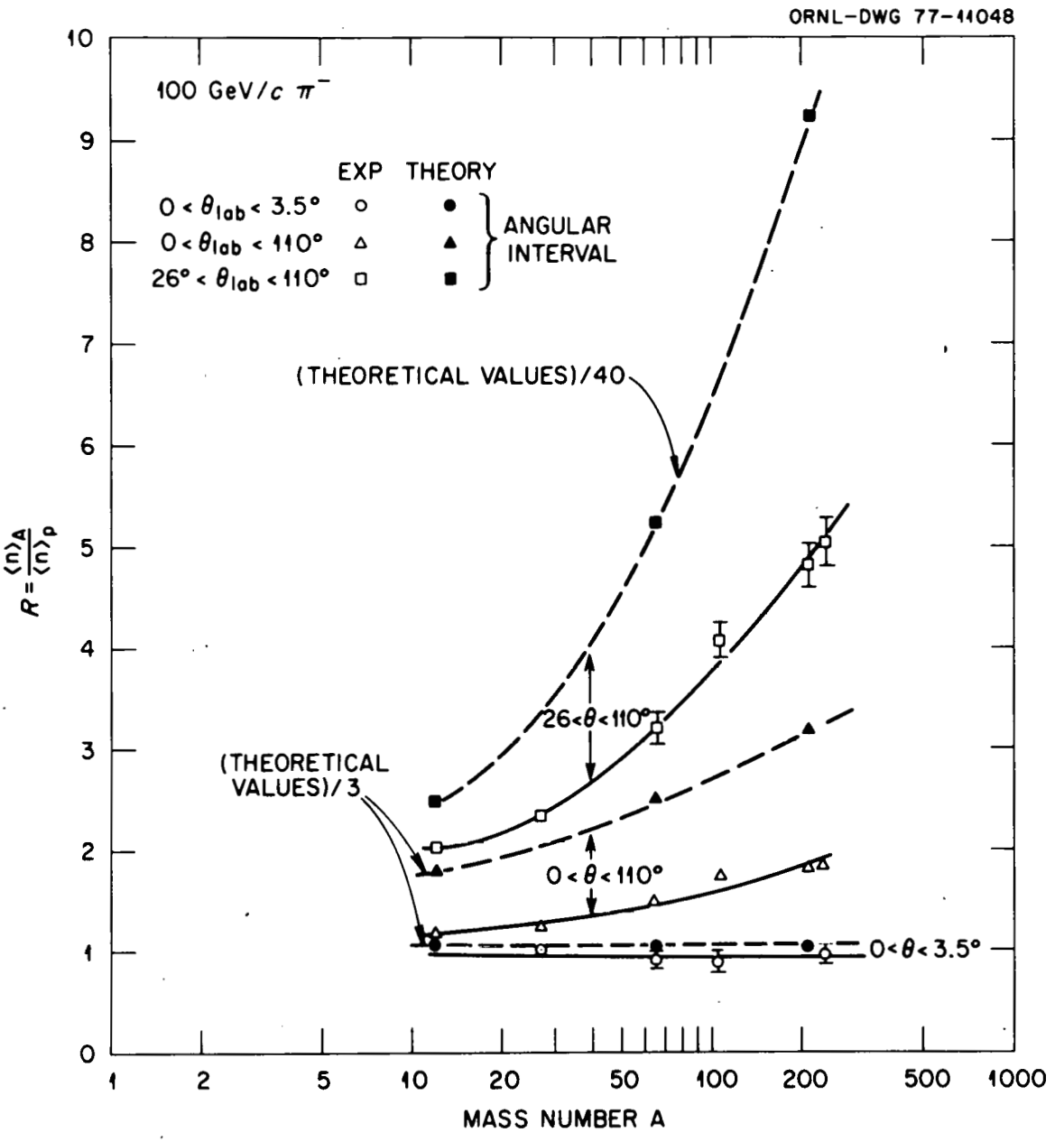

Fig. 12. Ratio of shower particles produced in various angular intervals from 100 GeV/c π^- on nuclei to those produced from 100 GeV/c π^- on p. The solid and dashed lines are drawn through the experimental and theoretical data respectively merely to guide the eye. $\beta \geq 0.85$ for the exp. data and ≥ 0.7 for the theoretical results. The theoretical values from the model have been divided by the values indicated. The statistical error on the theoretical results are of the order of the size of the symbols.

Table III. Theoretical values of the sum of the numbers of π^+ and π^- with $\beta \geq 0.7$ produced in various laboratory angular intervals from 100 GeV incident π^-

Lab. Angular Interval	Target C	Cu	Pb	P
0-3.5°	3.37±0.05	3.29±0.05	3.15±0.10	0.99
0-26°	8.15±0.11	9.99±0.13	11.73±0.27	1.86
0-110°	10.13±0.15	14.18±0.18	19.09±0.45	1.88
26°-110°	1.98±0.04	4.19±0.08	7.36±0.20	0.02

for the angular intervals 0-3.5° and 0-110° were arbitrarily divided by 3 and plotted, whereas the theoretical ratios for the angular interval 26-110° were divided by 40 before plotting.

Spectra

The spectra of secondary pions and protons at 13° and 45° from 33 GeV p on Al are shown in Figs. 13 and 14. The experimental data are not in absolute units but in units of particles/(sr GeV/c) per circulating proton.[21] All of the theoretical results, calculated in units of mb/(sr GeV/c), were arbitrarily divided by 2.5 for normalization purposes. The slopes of the pion and proton spectra, the relative magnitudes of pions to protons, and the change of these magnitudes with angle are fairly well represented by the theoretical predictions.

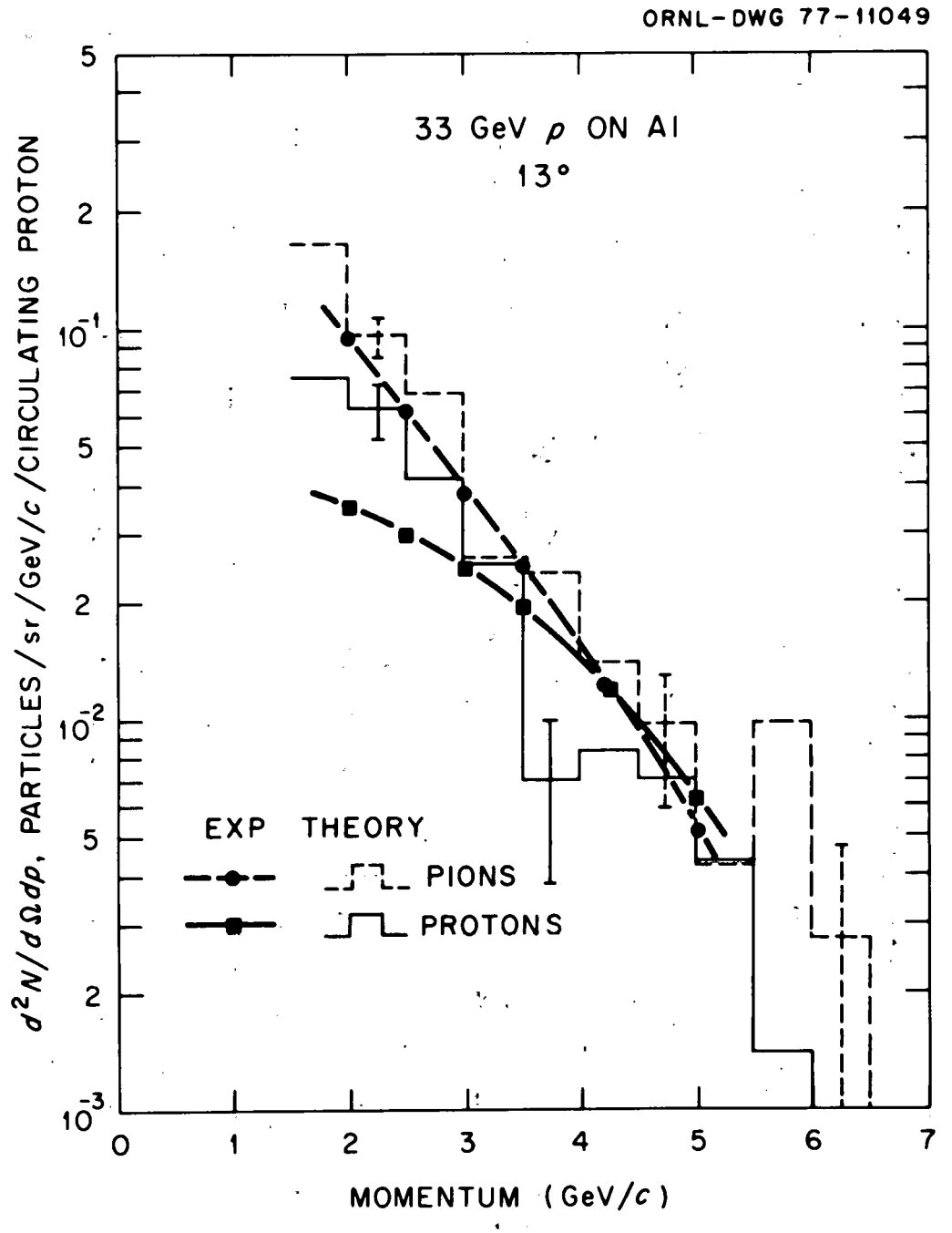

Fig. 13. Momentum spectra of pions and protons at a laboratory angle of 13° from 33 GeV p on Al. The experimental pion data represent either π^+ or π^- (their spectra are indistinguishable) and the experimental error bars for the pion and proton data are smaller than the symbols. The theoretical data are for π^+ and protons emitted into the angular interval 10-15°. Only representative statistical error bars are shown. The theoretical results, calculated in units of mb/(sr-GeV/c), have been arbitrarily divided by 2.5 for normalization purposes and plotted as shown.

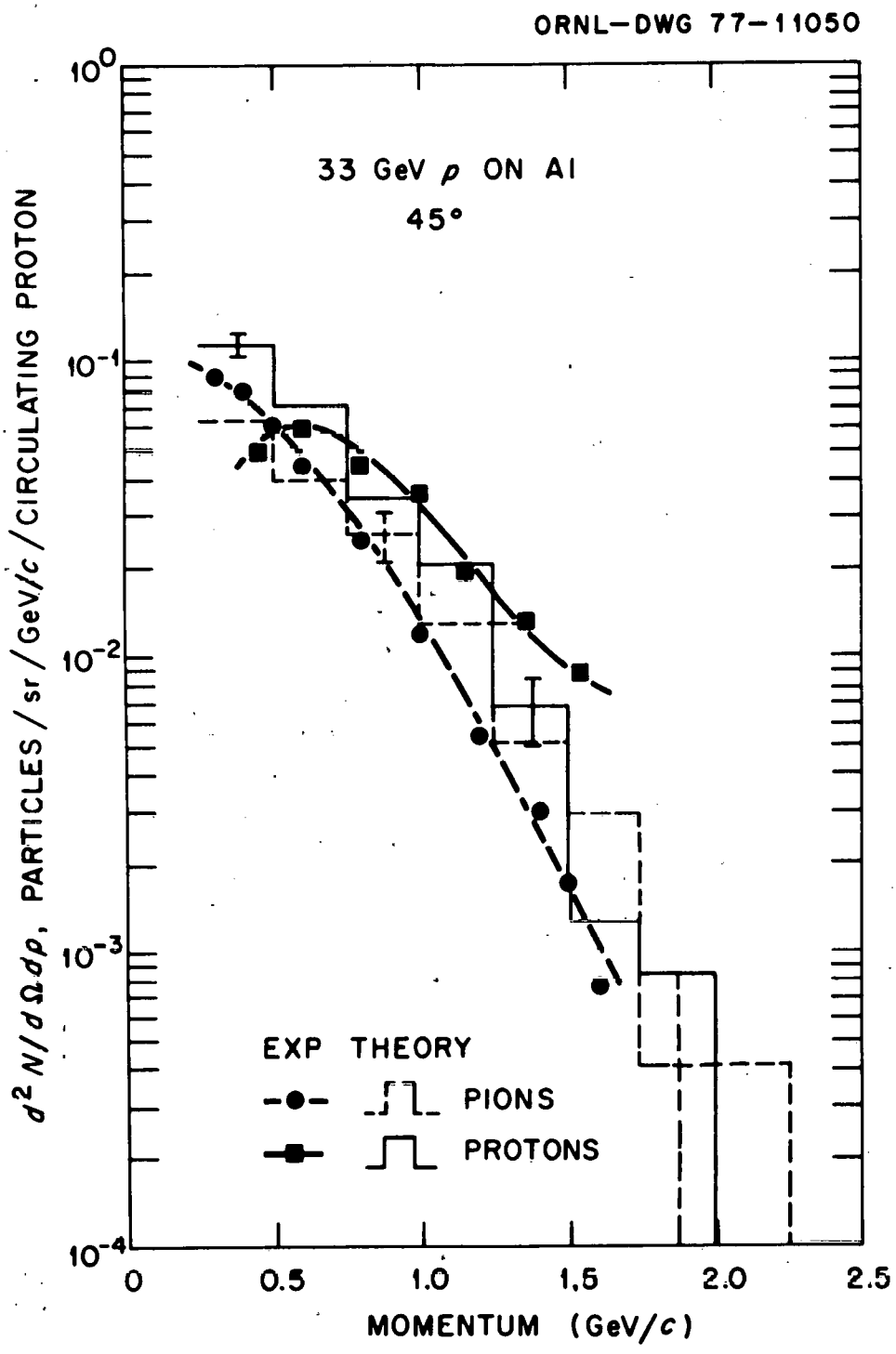

Fig. 14. Momentum spectra of pions and protons at a laboratory angle of 45° from 33 GeV p on Al. The theoretical results are for π^- and protons emitted into the angular interval 40-50°. Other details as in Fig. 13.

Radionuclides

The radionuclides produced from relatively low energy (11.5 GeV) protons interacting with cobalt were measured and compared to those produced from high energy protons (200 and 300 GeV), and it was found that the cross sections are essentially constant above 11.5 GeV.[22] Similar results were observed for silver[23] and uranium[24] targets. These results are consistent with those discussed above where the number of black tracks were shown to become independent of energy above $\sim$ 5 GeV, and they are indicative of a saturation effect of the excitation energy of the residual nucleus.

Calculations were performed for 11.5- and 300-GeV p on cobalt, and the results were compared with the experimental data of Katcoff *et al.*[22] The theoretical and experimental data are shown in Table 4. The agreement is reasonable for the cross sections from the interactions at 11.5 GeV, and essentially all of the ratios of the cross sections from the interaction at 300 GeV to those at 11.5 GeV are within the statistics of the experimental ratios. The saturation effect for the excitation energy is thus well reproduced by the theoretical model.

The absolute value of the experimental cross sections were evaluated under the assumption that the cross section for the monitor reaction, $^{27}Al(p,3pn)^{24}Na$, remained constant at 8.6 mb over the energy range of the experiments.[22] The calculated values for this cross section from the model were 7.7±2.0 mb at 11.5 GeV and 8.7±2.1 mb at 300 GeV, and hence no renormalization was necessary for these comparisons.

Table IV. Theoretical and experimental[a] cross sections for producing radionuclides from 11.5 GeV p on ^{59}Co, and also ratios of cross sections from 300 GeV p on ^{59}Co to those from 11.5 GeV p ($\sigma_{300}/\sigma_{11.5}$)

Nuclide	Mass No	$\sigma_{11.5}$(mb)		$(\sigma_{300}/\sigma_{11.5})^b$	
		Theor.	Exp.	Theor.	Exp.
Co	58	49.8±5.8	43±3	0.8±0.1	1.13±0.10
	57	16.1±3.3	20±2	0.9±0.3	1.10±0.12
	56	4.9±1.9	5.1±0.4	0.7±0.4	1.04±0.10
	55	0.7±0.7	0.66±0.10	--	1.02±0.17
Mn	54	10.5±2.7	19±2	0.9±0.3	1.06±0.12
	52	7.0±2.0	5.4±0.5	0.6±0.3	1.04±0.12
Cr	51	10.5±2.7	21±2	0.8±0.3	1.01±0.11
	48	1.4±1.0	0.28±0.02	0.5±0.5	0.93±0.08
V	48	9.1±2.5	9.4±0.7	0.6±0.3	1.00±0.09
Sc	48	0.0	0.60±0.07	--	0.95±0.12
	47	0.7±0.7	2.7±0.2	1.0±1.0	1.05±0.09
	46	3.5±1.6	6.7±0.5	1.0±0.6	1.01±0.09
	44	8.4±2.4	4.8±0.3	0.8±0.3	1.03±0.10
K	43	0.7±0.7	1.28±0.11	1.0±1.0	0.98±0.13
	42	2.8±1.4	3.9±0.5	0.5±0.4	0.85±0.12
Mg	28	0.0	0.51±0.04	--	1.06±0.11
Na	24	1.4±1.0	4.43±0.25	1.5±1.4	1.02±0.09
Be	7	0.0	10.2±1.1	--	1.15±0.17

[a] S. Katcoff *et al.*, Phys. Rev. Letters 30, 1221 (1973).

[b] Theoretical ratio is left blank if either σ_{300} or $\sigma_{11.5}$ are zero.

SUMMARY

An intranuclear cascade model for reactions of pions and nucleons with complex nuclei that should cover the energy range from $\sim$ 50 MeV to $\sim$ 1000 GeV has been developed. The model includes the effect of a diffuse nuclear surface, the Fermi motion of the bound nucleons within the nucleus, the exclusion principle, a local potential for nucleons, a localized reduction of the density of the nucleus during the development of the cascade, and the sequencing of the cascade events correctly with time. Since the model yields essentially the same results as earlier versions at low energy[3,4,10] ($\lesssim$ 3 GeV), comparisons were made with experimental data only at the higher energies to validate the model.

At energies $\sim$ 50 GeV the absolute value and the mass dependence of the reaction cross section for incident protons and pions calculated from the model are in good agreement with experimental data.

Over the energy range from $\sim$ 1-20 GeV, the predicted number of black tracks and the number of shower particles from pions on emulsion nuclei differ from experimental data by about a factor of 2 and $\sim$ 50%, respectively, at 5 GeV, but these differences decrease to about 15% for both types of tracks at 20 GeV. The energy dependences of the multiplicities of both track types are in good agreement with the experimental results, particularly in that the number of black tracks produced becomes independent of energy above 5 GeV.

The absolute value of the predicted shower particle multiplicities for 100 GeV pions on various nuclei is greater than the measured value by about 25% for light nuclei and greater by about 60% for heavy nuclei. The ratios of these multiplicities to those from protons are greater than

the experimental ratios by factors of 4 or 5. This results from the fact that the theoretical particle-proton model underestimates the number of shower particles produced per interaction. Replacing this model with a more realistic version will require considerable effort, but such a replacement, along with other modifications to improve the overall calculation, will be undertaken in the future. The effect of the inclusion of a more realistic particle-proton model is not clear. The calculated ratios of shower particles from nuclei to those from protons for 100-GeV incident pions varies by about a factor of 2 from carbon to lead whereas the experimental data show a variation of about 1.5 over the same mass range.

The energy dependence of these ratios for 10- to 1000-GeV protons on emulsions is well represented by the theoretical results.

A salient feature of the experimental data is that the shower-particle multiplicity in the forward direction is independent of target mass. The increase in the multiplicity with mass occurs mainly at large angles. This feature is fairly well reproduced by the theoretical model.

The agreement in absolute value between the theoretical predictions and the experimental data of the radionuclides produced from 11.5- and 3000 GeV p on cobalt is reasonable. More important is that the calculation predicts a relatively constant value for these cross sections over the energy range considered, which is in agreement with the experimental observations.

In short, the model overestimates the shower particle multiplicities by about 25% for high-energy reactions with light nuclei, and by about 60% for heavy nuclei. All other mass-dependent and energy-dependent trends that were investigated are predicted reasonably well.

COMPUTER CODE INFORMATION

The code HECC-1 (high energy cascade code, version 1) occupies 1210 K bytes in the IBM 360/91 computer. The running times for typical cases are given in Table 5. Note that these times are very sensitive to the cascade cutoff energy, i.e., the energy below which cascade histories are no longer followed.

Table V. Running times for HECC-1 on the IBM 360/91 for various cases

Inc. Particle Energy (GeV)	Cascade Cutoff Energy	Target	Minutes/(1000 Incident Particles)
100	0.056	C	7
11.5	0.0	Al	9
50	49	Al	0.5
300	0.0	Al	28
5	0.0	Br	15
5	0.056	Br	10
20	0.0	Br	29
20	0.056	Br	21
100	0.056	Br	48
1000	0.056	Br	110
100	0.056	Pb	102
200	0.056	Pb	150

THIS PAGE

WAS INTENTIONALLY

LEFT BLANK

REFERENCES

1. N. Metropolis, R. Bivins, M. Storm, Anthony Turkevich, and G. Friedlander, "Monte Carlo Calculations on Intranuclear Cascades. I. Low Energy Studies", Phys. Rev. 110, 185 (1958). N. Metropolis, R. Bivens, M. Storm, J. M. Miller, G. Friedlander, and Anthony Turkevich, "Monte Carlo Calculations on Intranuclear Cascades. II. High-Energy Calculations and Pion Processes", Phys. Rev. 110, 204 (1958).

2. M. P. Guthrie, "EVAP-4: Another Modification of a Code to Calculate Particle Evaporation from Excited Compound Nuclei", ORNL/TM-3119 (September 10, 1970). The basis of this model is that of I. Dostrovsky, Z. Fraenkel, and G. Friedlander, Phys. Rev. 116, 683 (1959).

3. Hugo W. Bertini, "Intranuclear Cascade Calculation of the Secondary Nucleon Spectra from Nucleon-Nucleus Interactions in the Energy Range 340 to 2900 MeV and Comparisons with Experiment", Phys. Rev. 188, 1711 (1969).

4. Hugo W. Bertini, "Nonelastic Interactions of Nucleons and π Mesons with Complex Nuclei at Energies Below 3 GeV", Phys. Rev. C6, 631 (1972).

5. Wit Busza, "Multiparticle Production in High Energy Hadron-Nucleus Collisions", pp. 211-236 in "AIP Conference Proceedings No. 26: International Conference on High-Energy Physics and Nuclear Structure - 1975" Series Editor Hugh C. Wolfe, (American Institute of Physics, NY 1975).

6. Luciano Bertocci, "Multiparticle Production on Nuclei: Theory", p. 238, AIP Conf. Proc. of the International Conference on High Energy Physics and Nuclear Structure - 1975 (American Institute of Physics, NY 1975).

7. K. Gottfried, "Space-Time Structure of Hadronic Collisions and Nuclear Multiple Production", Phys. Rev. Letters 32, 957 (1974).

8. M. Miescowicz, "Progress in Elementary Particle and Cosmic Ray Physics" Vol. X, 65 (1971); A. Z. Patashinskii, JETP Letters 19, 338 (1974).

9. I. Z. Artykov, V. S. Barashenkov, and S. M. Eliseev, "Inelastic Interactions of Cosmic Ray Particles with Atomic Nuclei at Very High Energies", Nucl. Phys. 87 241 (1966); I. Z. Artykov, V. S. Barashenkov, S. M. Eliseev, "Intranuclear Cascade Calculations of Many Particle Interactions", JINR-P2-3604 (1967), Joint Institute for Nuclear Research, Dubna, USSR; V. S. Barashenkov, K. K. Gudima, and V. D. Toneev, "Inelastic Interactions of High Energy Protons with Atomic Nuclei", Acta Physica Polonica 36, 887 (1969).

10. H. W. Bertini, Phys. Rev. 131, 1801 (1963).

11. K. Chen *et al.*, Phys. Rev. 166, 949 (1968).

12. K. Chen *et al.*, Phys. Rev. C4, 2234 (1971).

13. N. B. Gove *et al.*, "High Energy Nuclear Cascades: A Proposed Approach to Nuclear Simulations", Oak Ridge National Laboratory Report No. ORNL/TM-2627 (June 1969). The numerical approach was employed, p. 25. The momentum range $0\text{-}p_{Fermi}$ and the angular range $-1 \leq \mu \leq 1$ ($\mu = \cos\Theta$) were divided into 10 uniform intervals each.

14. Bruce G. Gibbard *et al.*, Phys. Rev. Letters 24 22 (1970).

15. D. Harting *et al.*, Nuovo Cimento 38 60 (1965).

16. R. M. Sternheimer and S. J. Lindenbaum, Phys. Rev. 123 333 (1961); 109, 1723 (1958); 105, 1874 (1957).

17. J. Ranft, Nucl. Inst. and Meth. 48, 133 (1967).

18. J. Ranft, CERN Report Nos. MPS/Int. MU/EP 66-3 (and 66-4) JR/ld 9.2.1966.

19. V. S. Barashenkov, K. K. Gudima, and V. D. Toneev, Acta Physica Pol. 36, 457 (1969).

20. W. Busza *et al.*, Phys. Rev. Letters 34, 836 (1975).

21. V. L. Fitch, S. L. Meyer, and P. A. Piroué, Phys. Rev. 126, 1849 (1962).

22. S. Katcoff *et al.*, Phys. Rev. Letters 30, 1221 (1973).

23. G. English, Y. W. Yu, and N. T. Porile, Phys. Rev. Letters 31, 244 (1973).

24. S. K. Chang and Nathan Sugerman, Phys. Rev. C9, 1138 (1974).

THIS PAGE

WAS INTENTIONALLY

LEFT BLANK

Appendix A

The high energy differential scattering cross section for nucleon-nucleon and pion-nucleon elastic scattering is represented by

$$\frac{d\sigma}{dt} = \exp[A-B|t|) = C\ e^{-B|t|} \tag{A1}$$

with

$$\cos \Theta_{cm} = 1 - \frac{|t|}{2K^2}\ , \tag{A2}$$

where Θ_{cm} is the polar angle of scattering in the cm system and

$$K^2 = \frac{M^4-2M^2(m_1{}^2+m_2{}^2)+(m_1{}^2-m_2{}^2)^2}{4M^2}\ . \tag{A3}$$

The symbol M represents the total energy in the cm system, and m_1 and m_2 represent the rest masses of the particles involved in the collision.

Because of the steepness of the experimental differential cross section curve vs Θ_{cm}, only scatterings in the forward hemisphere were considered, and the differential cross section was normalized to 1 over the interval $0 \leq \Theta_{cm} \leq 90°$, i.e.,

$$\sigma = \int_0^{2K^2} C\ e^{-B|t|}\ dt = 1\ , \tag{A4}$$

$$\therefore \qquad C = \frac{B}{1-e^{-2K^2B}}\ . \tag{A5}$$

Given a random number R, which is generated uniformly over the interval $0 \leq R \leq 1$, the value of t is sampled by solving

$$R = \int_0^{|t|} C\, e^{-B|t'|} dt' , \tag{A6}$$

for $|t|$, i.e.,

$$|t| = -\frac{1}{B} \ln[1-R+R\, e^{-2K^2B}] . \tag{A7}$$

The scattering angle in the cm system is then calculated from Eq. (A2). The azimuthal angle of scattering is selected from a uniform distribution over the interval $0 \leq \phi \leq 2\pi$.

Appendix B

B1. BASIC EQUATIONS

The pion-production model, the Ranft model,[18] has been modified slightly and incorporated in HECC-1, the first version of a high-energy intranuclear-cascade code described elsewhere. The pion-production model consists of four basic distributions which are functions of the total energy and emitted angle of the secondary particle. The slight modifications consist of representing the equations in terms of their energy dependence rather than their momentum dependence as given by Ranft. The reference frame is that in which the struck nucleon is at rest, and it is oriented such that the +z axis is in the direction of the incident particle.

The first basic function (Ref. 1, Eq. 9), unnormalized, is:

$$N_{nn}(E,\theta) = \left\{ \frac{A}{\sqrt{E_0^2 - m_n^2}} + \frac{B\sqrt{E^2 - m_n^2}}{E_0^2 - m_n^2} \left[1 + \sqrt{1 + \frac{E_0^2 - m_n^2}{m_n^2}} - \frac{\sqrt{E_0^2 - m_n^2}}{\sqrt{E^2 - m_n^2}} \sqrt{1 + \frac{E^2 - m_n^2}{m_n^2}} \right] \right\}$$

$$\times \left[1 + \sqrt{1 + \frac{E_0^2 - m_n^2}{m_n^2}} - \frac{\sqrt{E_0^2 - m_n^2}\sqrt{E^2 - m_n^2}}{m_n^2 \sqrt{1 + \frac{E^2 - m_n^2}{m_n^2}}} \right] \frac{(E^2 - m_n^2)\, E}{\sqrt{E^2 - m_n^2}} \exp[-C(E^2 - m_n^2)\, \theta^2] \ ,$$

where

$A = 0.55$,

$B = -0.30$,

$C = 2.68$,

E_0 = Total energy in GeV of the incident nucleon in the rest system of the struck nucleon,

E = Total energy in GeV of a secondary nucleon in the same system,

m_n = Nucleon mass in GeV,

θ = Polar angle in radians of the secondary nucleon measured from the incident-particle direction in the rest frame of the struck particle.

This distribution function gives the resulting nucleon total-energy spectrum when two nucleons collide and produce pions. When integrated over angles, the result is

$$N_{nn}(E) = \left\{ \frac{A\pi}{C\sqrt{E_0^2 - m_n^2}} + \frac{B\pi\sqrt{E^2 - m_n^2}}{C\sqrt{E_0^2 - m_n^2}} \left[1 + \sqrt{1 + \frac{E_0^2 - m_n^2}{m_n^2}} - \frac{\sqrt{E_0^2 - m_n^2}}{\sqrt{E^2 - m_n^2}} \sqrt{1 + \frac{E^2 - m_n^2}{m_n^2}} \right] \right\}$$

$$\times \left[1 + \sqrt{1 + \frac{E_0^2 - m_n^2}{m_n^2}} - \frac{\sqrt{E_0^2 - m_n^2}\sqrt{E^2 - m_n^2}}{m_n^2 \sqrt{1 + \frac{E^2 - m_n^2}{m_n^2}}} \right] \frac{E}{\sqrt{E^2 - m_n^2}} \quad .$$

The second basic distribution function (Ref. 1, Eq. 12), which applies to the secondary-pion-energy distribution in nucleon-nucleon production collisions, is:

$$N_{n\pi}(E,\theta) = \left\{ A_1(E^2 - m_\pi^2) \exp\left[- \frac{A_2\sqrt{E^2 - m_\pi^2}}{(E_0^2 - m_n^2)^{1/4}} - A_3(E_0^2 - m_n^2)^{1/4}\sqrt{E^2 - m_\pi^2}\,\theta^2 \right] \right.$$

$$\left. + \frac{B_1(E^2 - m_\pi^2)}{\sqrt{E_0^2 - m_n^2}} \exp\left[- B_2 \frac{E^2 - m_\pi^2}{E_0^2 - m_n^2} - B_3\sqrt{E^2 - m_\pi^2}\,\theta \right] \right\} \frac{E}{\sqrt{E^2 - m_\pi^2}} \quad ,$$

where

$A_1 = 4.75,$
$A_2 = 3.76,$
$A_3 = 4.23,$
$B_1 = 3.546,$
$B_2 = 10.21,$
$B_3 = 4.28,$

E_0 = total energy in GeV of incident nucleon in the rest system of the struck nucleon,

E = total energy in GeV of a secondary pion in the same system,

θ = polar angle in radians of the secondary pion measured from the direction of the incident nucleon in the rest system of the struck nucleon,

m_π = rest mass of the charged pion.

The constants A_2, A_3, B_2, and B_3 are those listed in Table III of Ref. 1. A_1 and B_1 were calculated as follows: A_1 (and similarly B_1) was assigned different values for π^+ and π^- in that table but no value was given for π°. The value of A_1 for π°'s was taken to be the average of the values for π^+ and π^-, but since the desired equation was to apply to all pions, the value taken for A_1 (and B_1) was the sum of the calculated value for π° plus the values tabulated for π^+ and π^-.

When this function is integrated over angles, the result is:

$$N_{n\pi}(E) = \left\{ \frac{A_1 \pi \sqrt{E^2 - m_\pi^2}}{A_3 (E_0 - m_n^2)^{1/4}} \exp\left[- A_2 \frac{\sqrt{E^2 - m_\pi^2}}{(E_0^2 - m_n^2)^{1/4}} \right] \right.$$

$$\left. + \frac{2\pi B_1}{B_3^2 \sqrt{E_0^2 - m_n^2}} \exp\left[- B_2 \left(\frac{E^2 - m_\pi^2}{E_0^2 - m_n^2} \right) \right] \right\} \frac{E}{\sqrt{E^2 - m_\pi^2}} \quad .$$

The third basic distribution function is arbitrarily taken to be

$$N_{\pi n}(E,\theta) \equiv N_{n\pi}(E,\theta),$$

but with m_π substituted for m_n and with m_n substituted for m_π. This function applies to the secondary-nucleon distribution in pion-nucleon collisions, and integrating over angles yields

$$N_{\pi n}(E) \equiv N_{n\pi}(E) ,$$

but with the roles of m_π and m_n reversed.

The fourth basic distribution function is again arbitrarily taken to be

$$N_{\pi\pi}(E,0) \equiv N_{n\pi}(E,0) ,$$

but with m_π substituted for m_n. This applies to the secondary-pion distribution for pion-nucleon collisions, and integrating over angles gives

$$N_{\pi\pi}(E) \equiv N_{n\pi}(E)$$

with m_π substituted for m_n.

B2. APPLICATION OF THE MODEL

In this section the general procedures for using the model are discussed. In the discussion, the term "energy" represents the total energy, and the relationship between energy E, momentum p, and kinetic energy T is

$$E_n = \sqrt{p_n^2 + m_n^2} = T_n + m_n$$

for a nucleon and

$$E_\pi = \sqrt{p_\pi^2 + m_\pi^2} = T_\pi + m_\pi$$

for a charged pion. For a neutral pion, m_{π° should be used in place of m_π.

The units for energy and mass are in GeV, and momentum is expressed in GeV/c. The masses are taken to be:

$$m_n = 0.9389 \text{ GeV},$$
$$m_\pi = 0.1396 \text{ GeV},$$
$$m_{\pi^\circ} = 0.1350 \text{ GeV}.$$

In the following sampling technique, tests on energy and charge are made to be sure that total energy and charge can always be conserved before the last particle is selected. The last particle then is selected so that energy and charge are conserved. Provisions are made so that at least one pion is created in the interaction. For the secondary-nucleon and -pion distributions in a nucleon-nucleon collision, the procedure is as follows:

1. The variable INCH is set equal to the sum of the charges of the colliding nucleons. A pion or a nucleon is selected, each with a probability of one-half:
   a. If a pion is selected, the energy E_{π_1} is selected from $N_{n\pi}(E)$ and tested to ensure that there is sufficient energy remaining

in the reaction to produce at least two nucleons; i.e., $E_{\pi_1} \leq (E_0 + m) - 2m$ is tested. If the test fails, a new E_{π_1} is sampled. With a probability of one-third, the charge of the pion [$CH(\pi_1)$] is set equal to +1, 0, or -1, and the test $INCH - 2 \leq CH(\pi_1) \leq INCH$ is made. If the test fails, a new pion charge is sampled. The angle θ is sampled from $N_{n\pi}(E_{\pi_1},\theta)$ and an azimuthal angle ϕ is selected from $d\phi/2\pi$. This completely specifies the selected pion.

b. If a nucleon is selected, the nucleon energy E_{n_1} is sampled from $N_{nn}(E)$ and tested to be sure that there is sufficient energy to produce another nucleon and at least one pion; i.e., $E_{n_1} \leq (E_0 + m) - m - m_\pi$ is tested, with new E_{n_1}'s sampled from $N_{nn}(E)$ until the test is passed. With a probability of one-half, the charge of the nucleon is set to +1 or zero. Letting the variable CH equal this value, the test $INCH - 2 \leq CH(n) \leq INCH + 1$ is made.* If the test fails, a new charge is selected until the test is passed. The polar angle θ is selected from $N_{nn}(E_{n_1},\theta)$ and the azimuthal angle ϕ is selected from $d\phi/2\pi$. This completely specifies the selected nucleon.

---

*The point of the tests on the charge is to be sure that charge can be conserved if the minimum number of particles is selected for the interaction. For a nucleon-nucleon reaction, the minimum number is two nucleons plus one pion. For a pion-nucleon reaction, it is two pions plus one nucleon.

2. With a probability of one-half, a nucleon or a pion is selected:
   a. If a pion, the procedure similar to 1.a is carried out. Tests on energy and charge are made so that one can ultimately include the selection of two nucleons and also that charge can be conserved.
   b. If a nucleon, similar comments apply. One must have at least two nucleons and one pion in a nucleon-nucleon collision.
3. After two nucleons have been selected, the remaining particles are chosen to be pions.
4. Given that at least the minimum number of particles have been selected, the sampling procedure terminates when the energy of a particle is selected such as to preclude the production of an additional pion; i.e.,

$$(E_0 + m) \geq \sum_j E_j > (E_0 + m) - m_\pi \quad ,$$

where E_j is the total energy of the jth selected particle. The energy of the last particle is assigned an energy such that total energy is conserved, and its charge is such that charge is conserved.

5. A vector $\bar{V}$ is calculated from

$$\bar{V} = \bar{p}_0 - \sum_j \bar{p}_j$$

($\bar{p} \equiv$ momentum), and the momentum of the last selected particle is assigned a direction along $\bar{V}$. Momentum is not conserved in general, but the direction of the last particle is taken to be that which would conserve momentum if the magnitude of its momentum were correct.

For the secondary-nucleon and -pion distributions in a pion-nucleon reaction, the procedure is similar to that described above, where now the distributions $N_{\pi n}(E,\theta)$ and $N_{\pi\pi}(E,\theta)$, and their integrals over θ, are used.

B3. SAMPLING TECHNIQUE

One must sample the secondary-particle energy E from the distribution functions $N_{nn}(E)$, $N_{n\pi}(E)$, $N_{\pi n}(E)$, and $N_{\pi\pi}(E)$ to obtain E, given E_0. One then must sample from $N_{nn}(E,\theta)$ or $N_{n\pi}(E,\theta)$, etc., to get θ, given E and E_0. The following method is used: At each value of E_0 listed below, normalized distribution functions are calculated and defined by:

$$f_{nn}(E,E_0) = \frac{N_{nn}(E,E_0)}{\int_{m_n}^{E_0} N_{nn}(E,E_0)\,dE} ,$$

$$f_{n\pi}(E,E_0) = \frac{N_{n\pi}(E,E_0)}{\int_{m_\pi}^{E_0} N_{n\pi}(E,E_0)\,dE} ,$$

$$f_{\pi n} = \text{etc.} ,$$

$$f_{\pi\pi} = \text{etc.}$$

The following values of E_0 for each function are used. The numerals added to the masses are the relative kinetic energies of the incident particles. (Note: The Ranft model is employed only when the relative kinetic energy is > 2.5 GeV in a nucleon-nucleon collision and > 1.5 GeV in a pion-nucleon collision.)

f_{nn} and $f_{n\pi}$	$f_{\pi n}$ and $f_{\pi\pi}$
$E_0 = 2.5 + m_n$	$E_0 = 1.5 + m_\pi$
$E_0 = 5.0 + m_n$	$E_0 = 3.0 + m_\pi$
$E_0 = 7.5 + m_n$	$E_0 = 5.0 + m_\pi$
$E_0 = 10 + m_n$	$E_0 = 7.5 + m_\pi$
$E_0 = 15 + m_n$	$E_0 = 10 + m_\pi$
$E_0 = 20 + m_n$	$E_0 = 15 + m_\pi$
$E_0 = 25 + m_n$	$E_0 = 20 + m_\pi$
$E_0 = 30 + m_n$	$E_0 = 25 + m_\pi$
$E_0 = 40 + m_n$	$E_0 = 30 + m_\pi$
$E_0 = 50 + m_n$	$E_0 = 40 + m_\pi$
$E_0 = 100 + m_n$	$E_0 = 50 + m_\pi$
$E_0 = 500 + m_n$	$E_0 = 100 + m_\pi$
$E_0 = 1000 + m_n$	$E_0 = 500 + m_\pi$
$E_0 = 1500 + m_n$	$E_0 = 1000 + m_\pi$
$E_0 = 2000 + m_n$	$E_0 = 1500 + m_\pi$
$E_0 = 3000 + m_n$	$E_0 = 2000 + m_\pi$
	$E_0 = 3000 + m_\pi$

At each value of E_0 and for each distribution function, the solutions E to the equations of the type

$$R = \int_m^E f(E)\, dE \qquad (1)$$

are tabulated for uniform intervals of R ranging from 0 to 1. The following number of uniform intervals of R for each E_0 are given below. (Note: The number of values of E in each table is one more than the number of intervals.)

E_0	No. of Intervals
1.5 + m	6
2.5 + m	10
3.0 + m	12
5.0 + m	10
7.5 + m	15
10 + m	10
15 + m	10
20 + m	10
25 + m	12
30 + m	15
40 + m	20
50 + m	20
100 + m	20
500 + m	50
1000 + m	100
1500 + m	100
2000 + m	100
3000 + m	100

To sample an energy E of the secondary particles from the energy distributions for a reaction, one calculates E_r for that reaction,* generates a random number R, and finds, by linear interpolation, values of E corresponding to R for the tabulated E_0 energies that bracket the calculated E_r. Then by interpolating linearly in energy between these corresponding values of E, one can obtain E at the E_r for the reaction.

For each of the secondary-particle energies E listed in the tables, where E is the solution to Eq. 1, eleven values of θ were tabulated. Each θ is a solution to

$$R = \frac{\int_0^{\theta} N(E,\theta)\, d\theta}{\int_0^{\theta_{max}} N(E,\theta)\, d\theta} \qquad (2)$$

for eleven uniform values of R from 0 to 1. The integrations were carried out numerically. The value of θ_{max} varied with the distribution used (i.e., N_{nn}, $N_{n\pi}$, etc.) and varied with E for each distribution. The value of θ_{max} was determined as that value beyond which contributions to the integral were negligible (10^{-6} %).

*E_r is the total energy of the particle initiating the reaction.

To assist in the understanding of the sampling technique for θ, the manner in which the data are tabulated is illustrated schematically below.

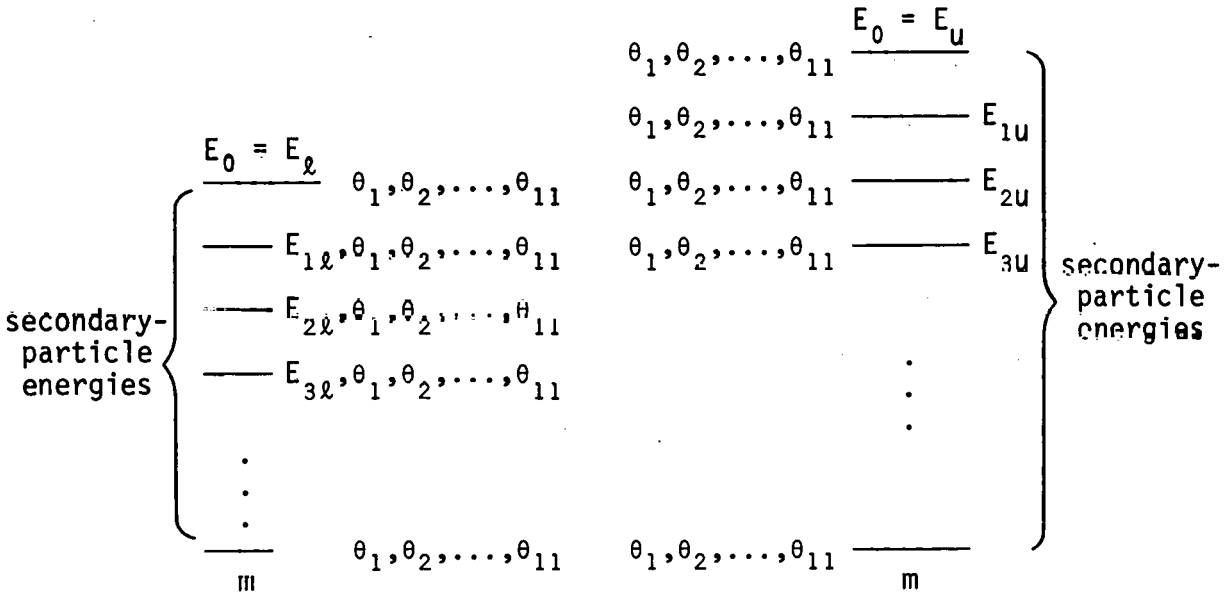

Eleven values of θ are tabulated for each tabulated secondary-particle energy E_i. The values of θ are solutions to Eq. 2 as described above.

In the computer program, the angle θ is sampled along with the secondary-particle energy. Call this secondary-particle energy E_s and let the total energy of the particle initiating the reaction be E_r. As mentioned above, the tabulated values of E_0 that bracket E_r are determined. For each of these E_0's, the tabulated values of E are found that bracket the solution to

$$R = \int_m^E f(E)\, dE \quad , \tag{1}$$

where R is the random number that was generated to select E_s. Another random number is generated and a θ is found by linear interpolation for each of the tabulated E's that brackets the solution to Eq. 1. A θ is found by interpolating linearly between the tabulated E's in the same manner that the solutions

to Eq. 1 are found. One then has the values of E corresponding to R (Eq. 1) for each of the bracketing E_0's, and, along with each E, the corresponding θ's. By interpolating linearly in energy between the E_0's, the value of E_s and the associated value of θ are determined. The exception to the above procedure is that Lagrangian interpolation rather than linear interpolation is used for θ in determining the θ's for the tabulated E's when the random number generated to select the θ's falls between 0 and 0.1.

THIS PAGE

WAS INTENTIONALLY

LEFT BLANK

Internal Distribution

1. M. P. Guthrie
2. L. S. Abbott
3. F. S. Alsmiller
4. R. G. Alsmiller, Jr.
5-19. H. W. Bertini
20. H. P. Carter
21-26. A. H. Culkowski
27. T. A. Gabriel
28. N. B. Gove
29. O. W. Hermann
30. F. C. Maienschein
31. F. R. Mynatt
32. E. M. Oblow
33. R. W. Roussin
34. RSIC
35. R. T. Santoro
36. M. L. Tobias
37. C. R. Weisbin
38. A. Zucker
39. P. Greebler (Consultant)
40. W. W. Havens, Jr. (Consultant)
41. A. F. Henry (Consultant)
42. R. E. Uhrig (Consultant)
43-44. Central Research Library
45. ORNL Y-12 Technical Library, Document Reference Section
46-47. Laboratory Records Department
48. ORNL Patent Office

External Distribution

49. R. Fricken, Division of Physical Research, U.S. Energy Research and Development Administration, Washington, DC 20545.
50. H. Goldstein, Columbia University, 287A Mudd Building, New York, NY 10027.
51-77. Technical Information Center (TIC).
78. U.S. ERDA Oak Ridge Operations, Research and Technical Support Division, P.O. Box E, Oak Ridge, TN 37830: Director.
79-127. Given High-Energy Accelerator Shielding distribution.